Latvijas Universitātes Cietvielu fizikas institūts
Institute of Solid State Physics, University of Latvia

AB INITIO SIMULATIONS OF PERFECT AND DEFECTIVE INORGANIC NANOTUBES AND NANOWIRES

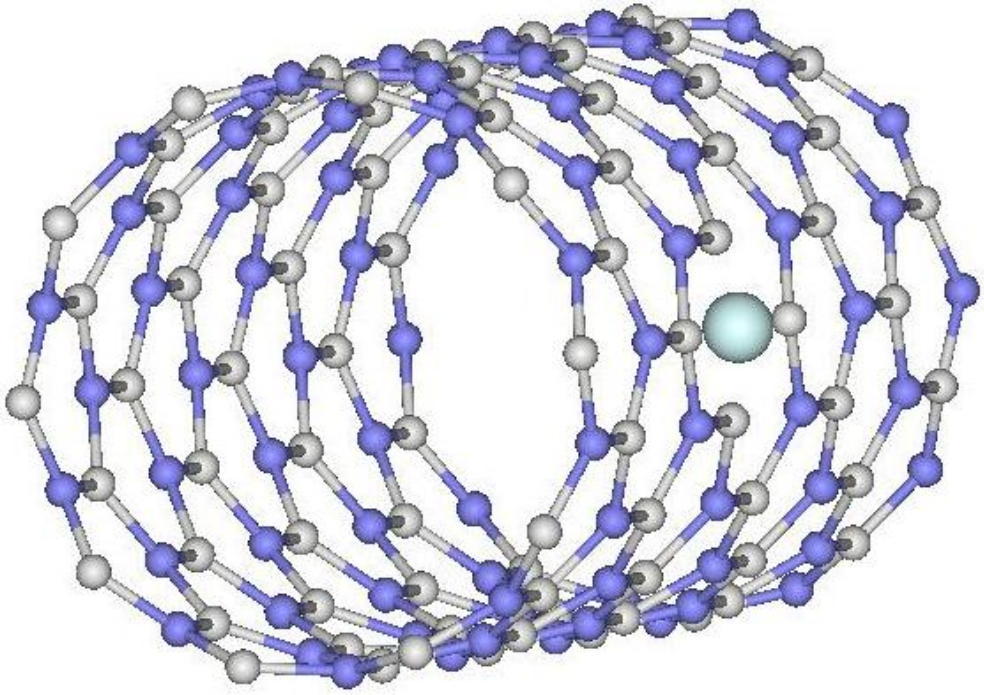

Yu.F. Zhukovskii[1], S. Piskunov[1,2,3],

[1]Latvijas Universitātes Cietvielu fizikas institūts, Rīga, Latvija;

[2]Latvijas Universitātes Fizikas un matematikas fakultāte, Rīga, Latvija;

[3]Latvijas Universitātes Datorikas fakultāte, Rīga, Latvija

BSANS, Riga, Latvia, 2 October, 2012

Outline

1. STRATEGY FOR THEORETICAL STUDY OF 1D NANOSTRUCTURES AND THEIR MAIN CLASSES

2. COMPUTATIONAL DETAILS OF DFT-LCAO CALCULATIOMS ON ELECTRONIC STRUCTURE

3. Models and properties of perfect BN, TiO_2 and $SrTiO_3$ SW NTs

4. Models and properties of perfect BN and TiO_2 DW NTs

5. Models and properties of defective BN, TiO_2 and $SrTiO_3$ SW NTs

6. Models and properties of perfect TiO_2 NWs

7. SUMMARY AND PREDICTIONS

1. STRATEGY FOR THEORETICAL STUDY OF NANOSTRUCTURES AND THEIR MAIN CLASSES

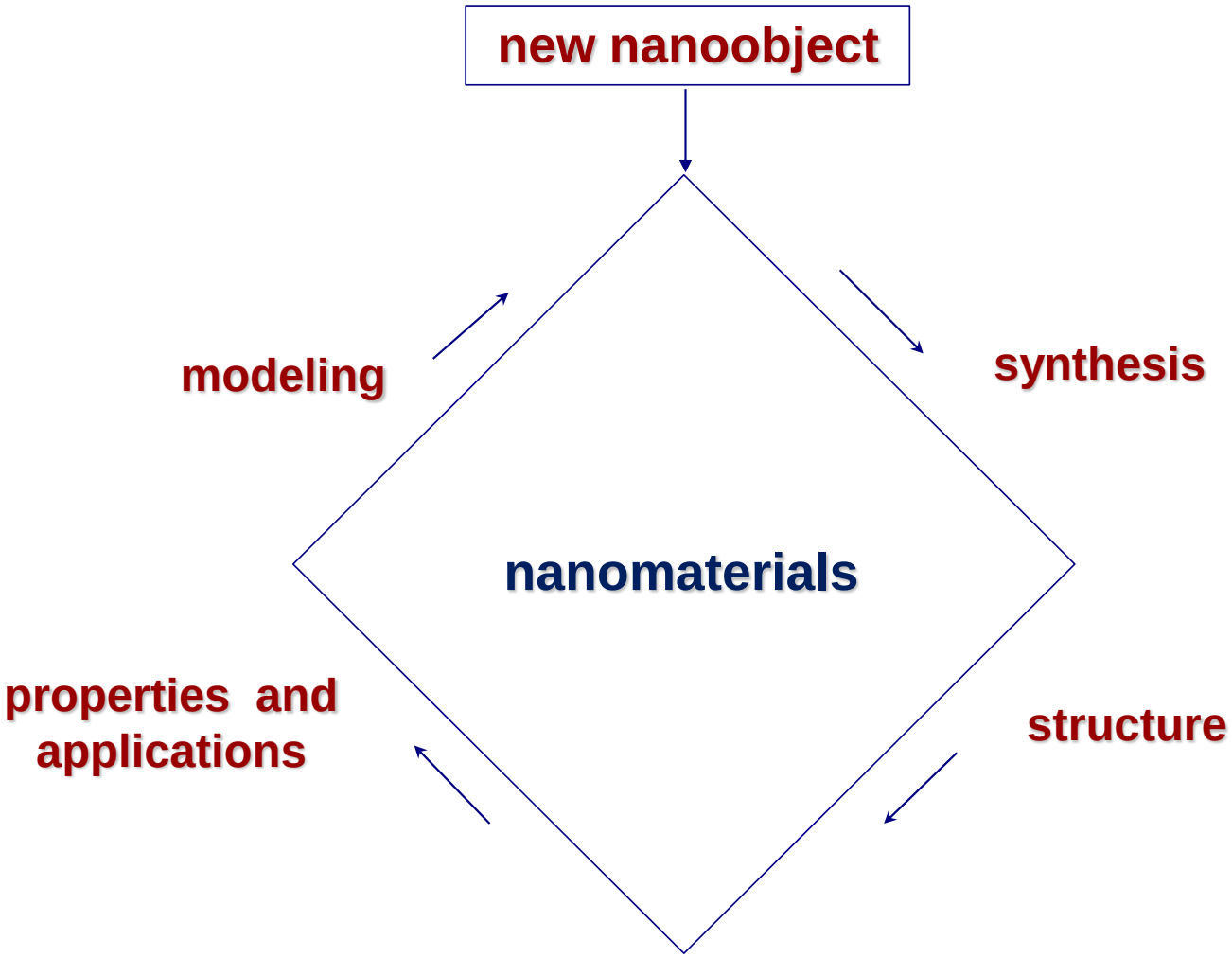

Why neutrons?

- Penetrating power
- Light- and similar-element capability
- Range of sample environments

Nobel Prize in Physics 1994 - Shull and Brockhouse

Neutrons show where atoms are…..

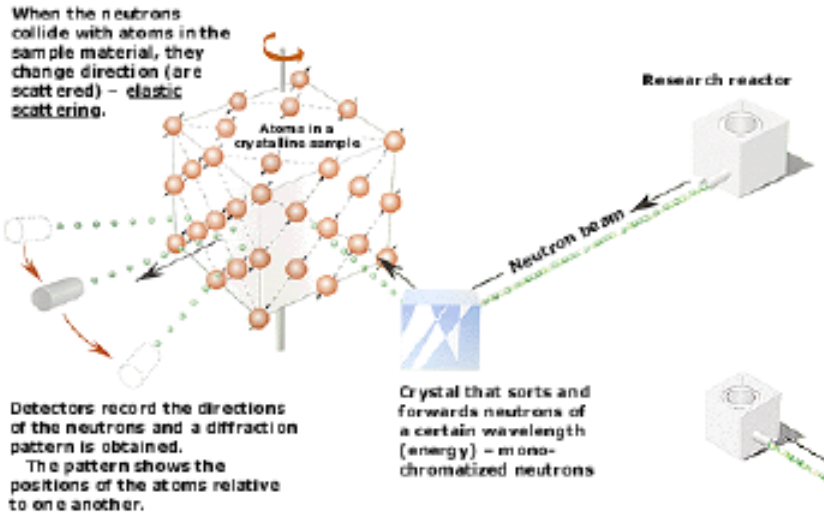

… and what atoms do

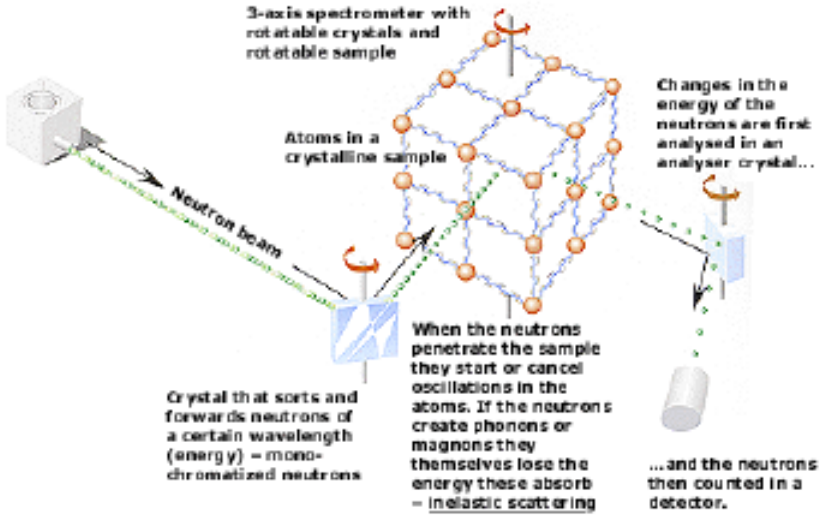

Neutrons measure structure and dynamics

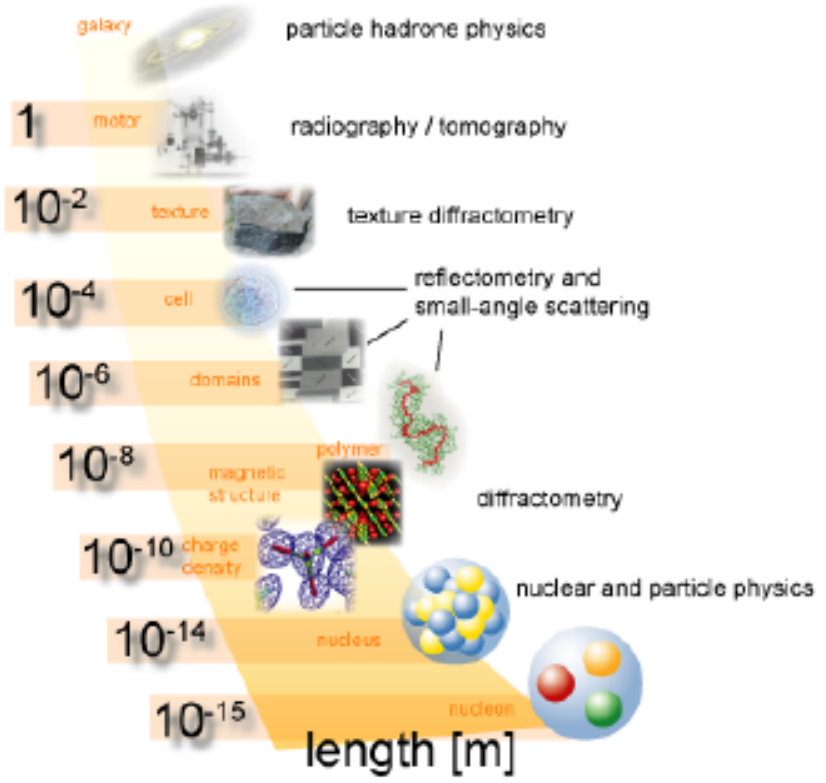

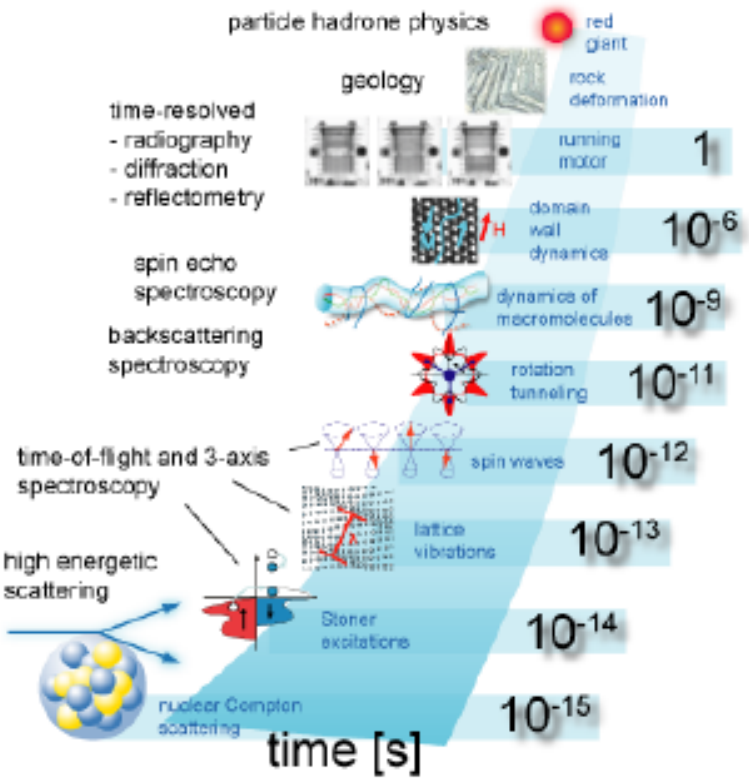

OBSERVED NANOSTRUCTURES

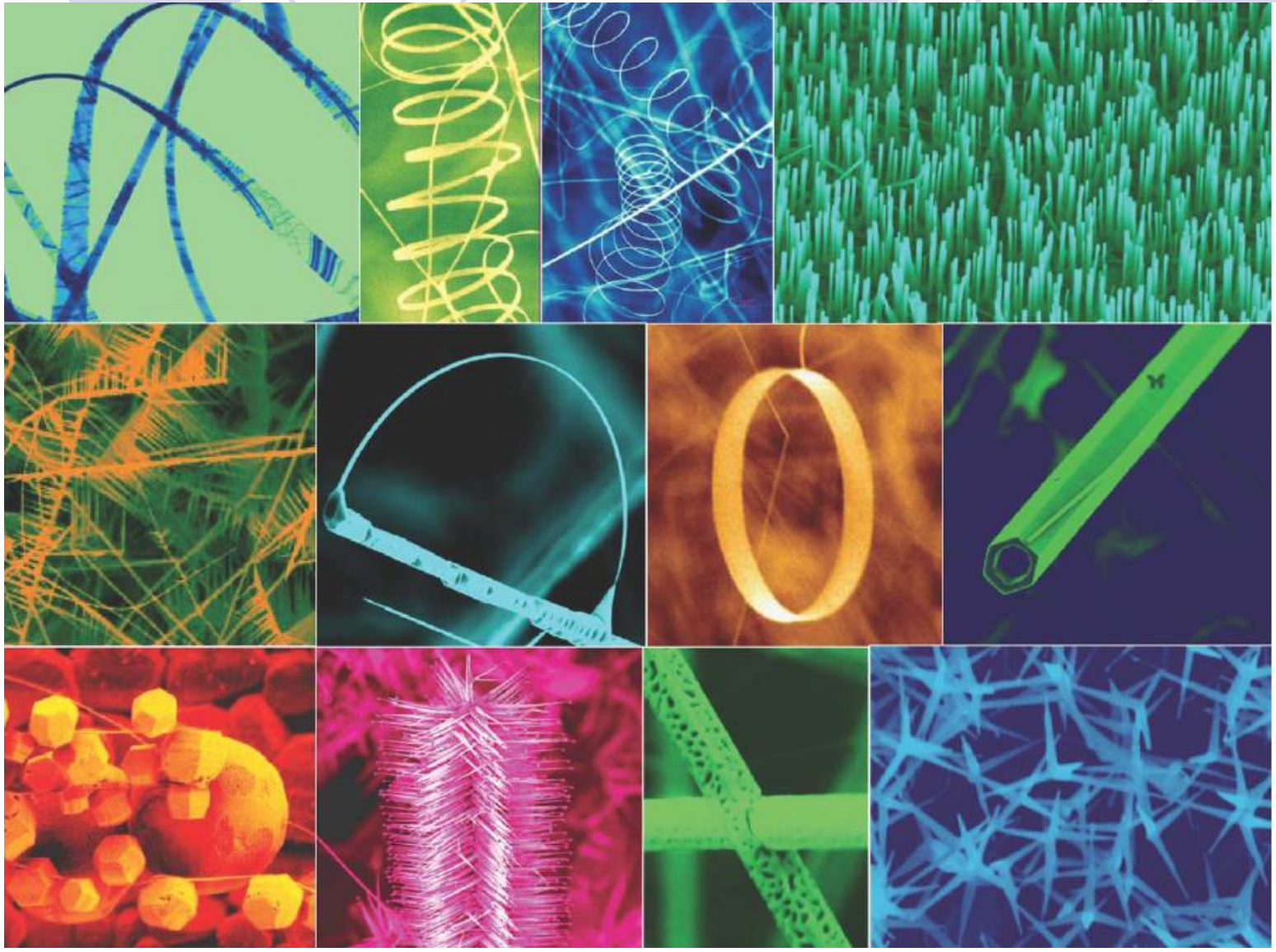

CLASSIFICATION OF 1D NANOSTRUCTURES

Nanostructure is defined formally as the structure at least one size of which (d) is less or equal to a critical one (d^*): $d < d^* \approx 10^2$ nm. Theoretical simulations on various types of 1D nanostructures, including their hybrid morphologies, for different classes of inorganic substances (*e.g.*, carbon) are widely developing during the last two decades.

There are three main types of models for 1D periodic nanostructures simulating really synthesized samples, which size along the translation axis overwhelmingly exceeds the sizes along the other two directions ($l >> d_i$):

(i) mono- and multi-layer nanoribbons, nanobelts, nanohelices, *etc.;*

(ii) single- and multi-wall nanotubes, nanoscrolls, *etc.*;

(iii) densely-packed nanowires, nanofibres, nanoneedles, *etc.*

We consider mainly those nanostructures which shapes and internal morphologies are highly-symmetric and, thus, may be more effectively described theoretically. Indeed, for their atomistic calculations, there is quite enough to consider only part of the whole ensemble of atoms (which corresponds to irreducible presentations). In reality, distortion of these symmetric structures can make them more preferable energetically, especially in conditions of room and higher temperature, various gaseous media, irradiation, electric and magnetic fields, *etc*. A number of atomistic models for nanostructures are considered here, including description of their properties.

MAIN 1D NANOSTRUCTURES FOR MODELING

NANORIBBONS

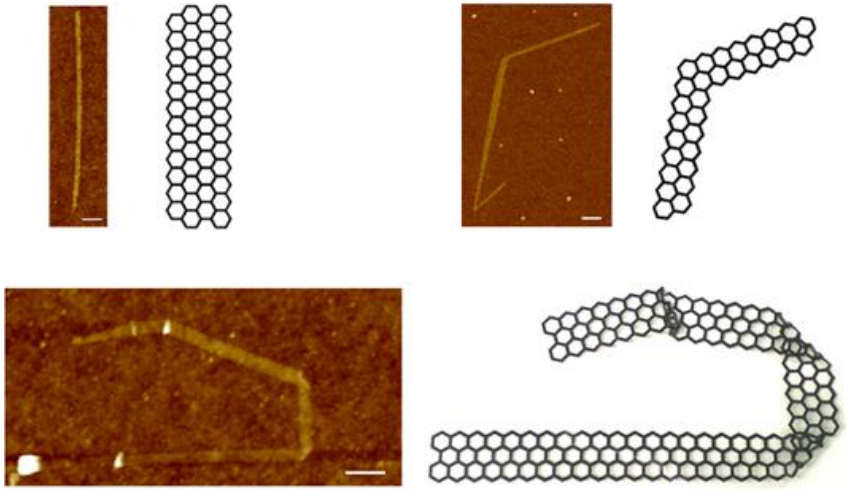

NANOWIRES

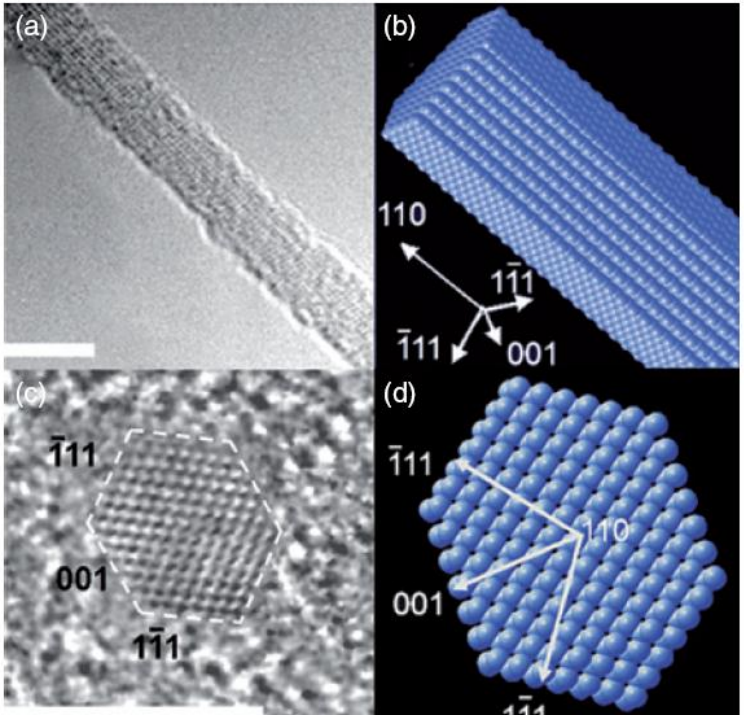

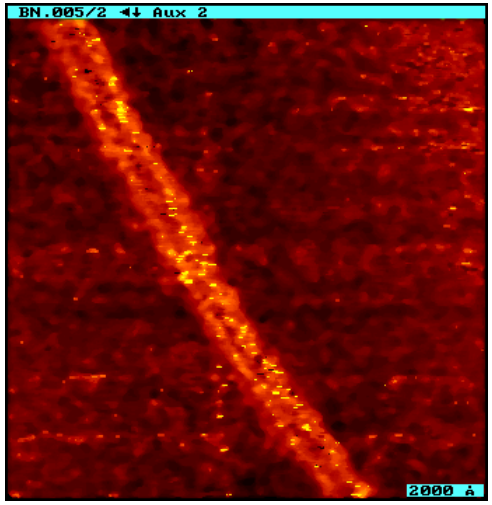

NANOTUBES

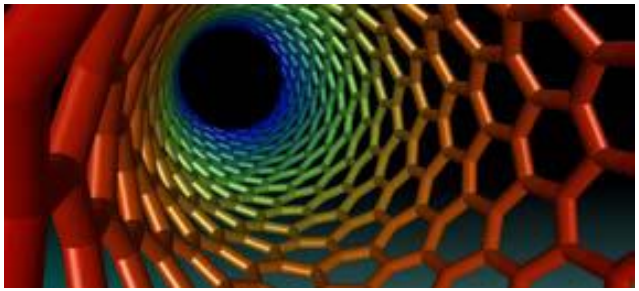

RELATED 1D NANOSTRUCTURES

MULTI-WALL NANOTUBE

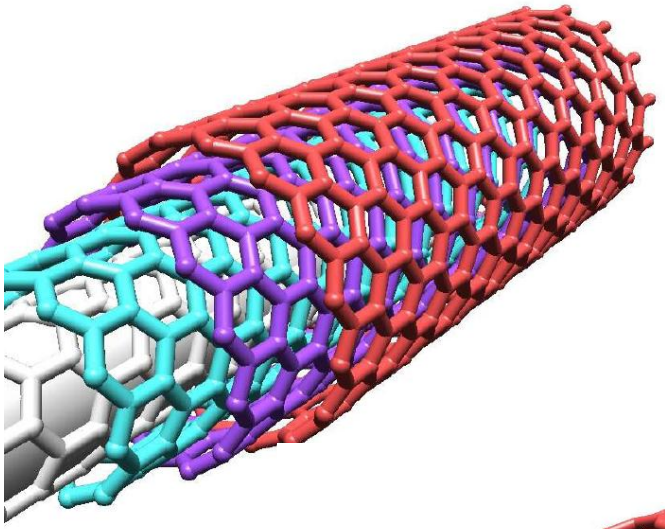

BUNDLE OF SINGLE-WALL NANOTUBES

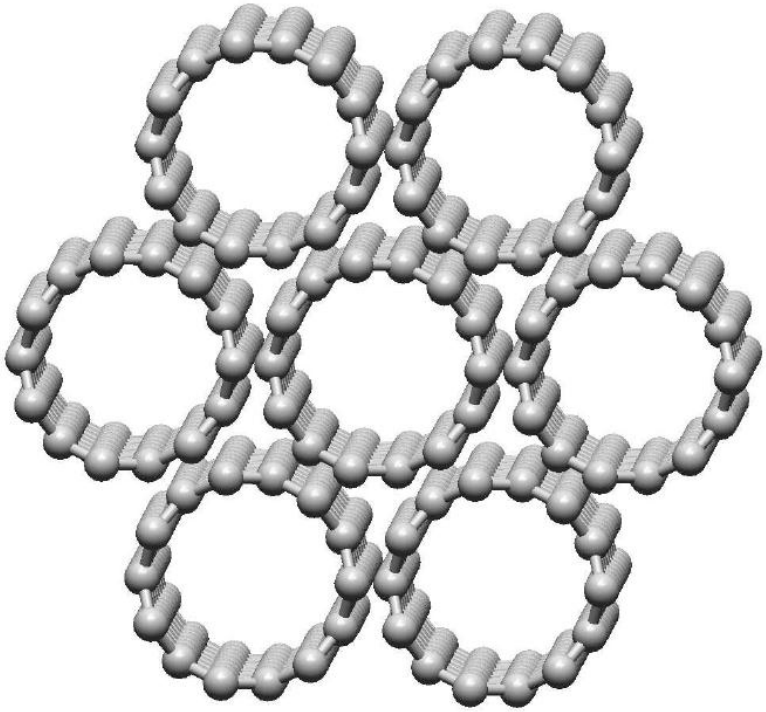

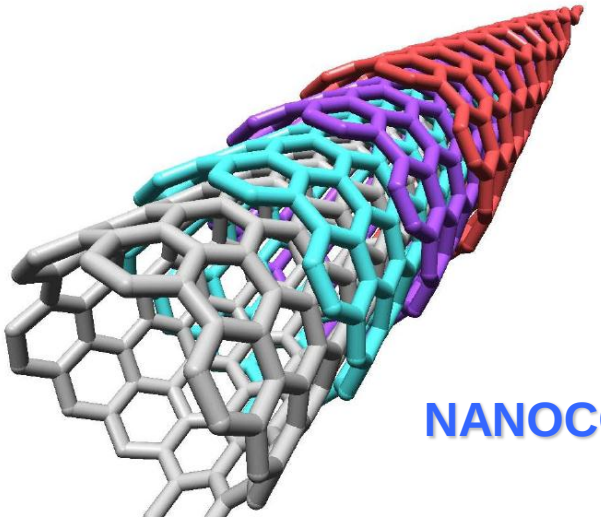

NANOCONE STACK

MODEL OF 2D → 1D TRANSITION FOR SIMPLEST NANOSTRUCTURE

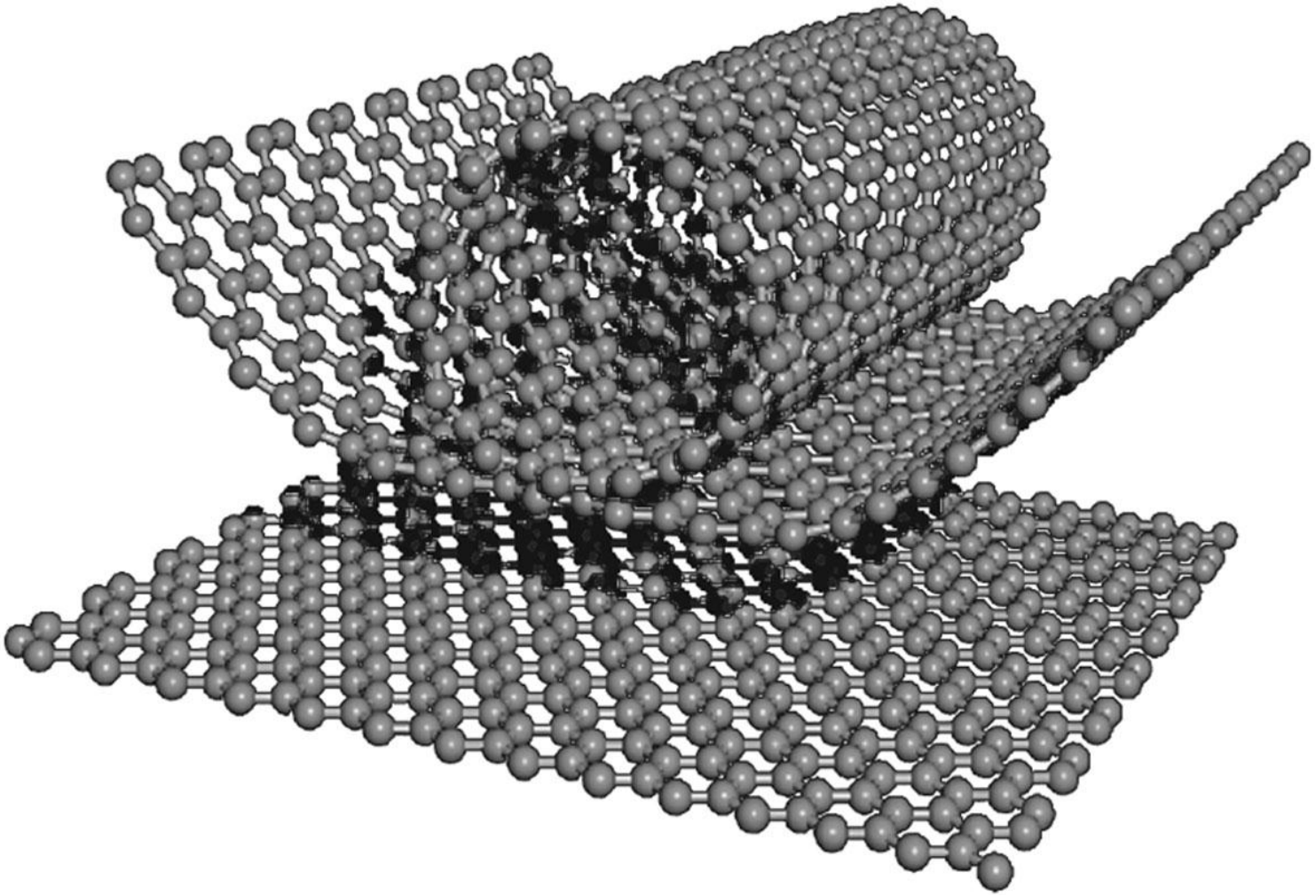

GRAPHENE SHEET AND ITS ROLLING UP TO CARBON NANOTUBE

1D-3D HYBRID NANOSTRUCTURES

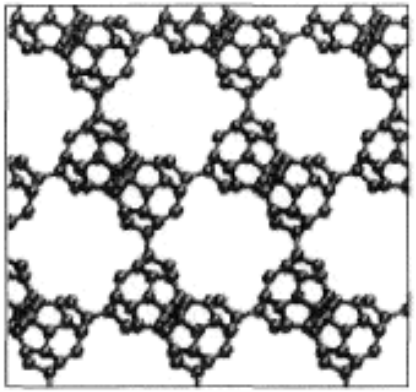

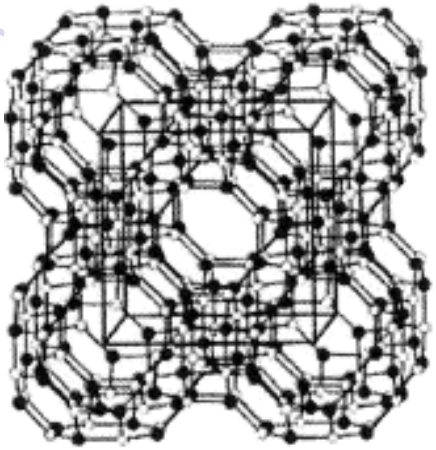

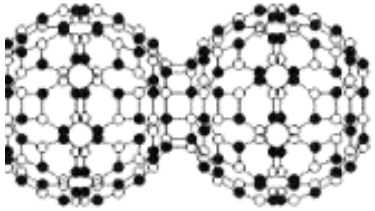

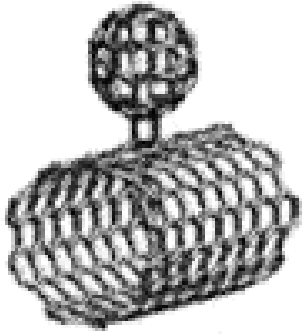

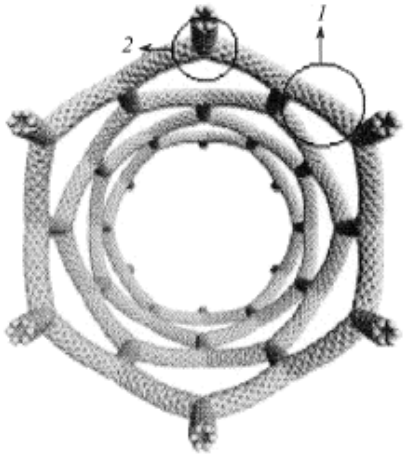

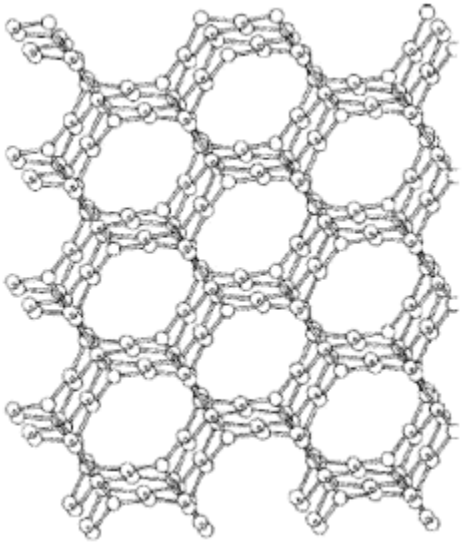

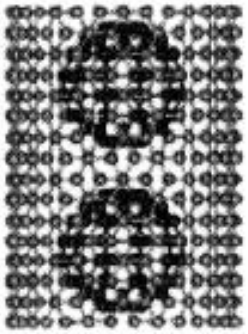

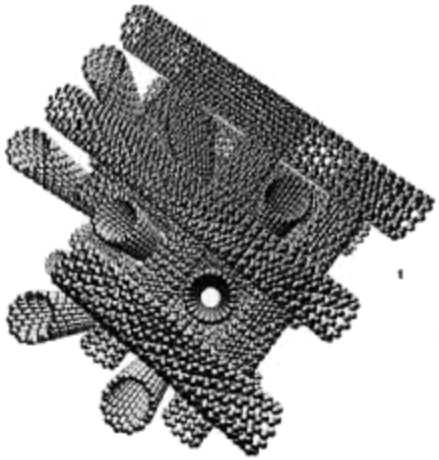

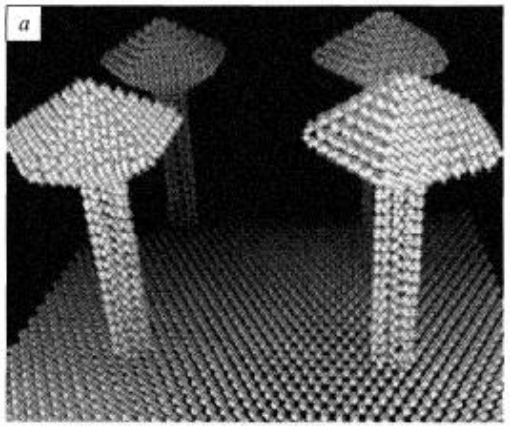

R.A. Evarestov, Yu.F. Zhukovskii

Quantum Chemistry of Monoperiodic Systems

The First-principles Treatment of Inorganic Nanotubes, Nanoribbons and Nanowires

Springer
Berlin Heidelberg New York
Hong Kong London
Milan Paris Tokyo

2. COMPUTATIONAL DETAILS

DFT-LCAO METHOD

The first principles DFT-LCAO method, as implemented in the *CRYSTAL-09* code elaborated at the University of Torino,[1] allows us to describe nanotubes and other 1D nanostructures in their original space form, unlike the Plane-Wave methods, which are quite widespread nowadays for *ab initio* calculations on low-dimensional periodic systems.

Our calculations on DW NTs have been performed using the hybrid Hartree-Fock/Kohn-Sham (HF/KS) exchange-correlation Hamiltonian PBE0 by Perdew-Becke-Erzerhof[2] combining exact HF non-local exchange and KS exchange operator within the Generalized Gradient Approximation (GGA) as implemented in *CRYSTAL-09* code.

1. Dovesi, R.; Saunders, V. R.; Roetti, C.; Orlando, R.; Zicovich-Wilson, C. M.; Pascale, F.; Civalleri, B.; Doll, K.; Harrison, N. M.; Bush, I. J.; D'Arco, Ph.; Llunell, M. *CRYSTAL-2009 User Manual*: University of Turin: Turin 2009.
2. Ernzerhof, M.; Scuseria, G.E. *J. Chem. Phys.* **1999**, 110, 5029–5036.

2. *CRYSTAL* calculations: localized crystalline orbitals

CRYSTAL-09 package is widely used now to perform comprehensive *ab initio* LCAO periodic calculations. Both *HF* and *DFT methods* implemented in this codes are realized *via* the self-consistent field (*SCF*) solution of the one-electron equations:

$$\hat{h}_i \varphi_{\mathbf{k}i}(\mathbf{r}) = \varepsilon_{\mathbf{k}i} \varphi_{\mathbf{k}i}(\mathbf{r}) \ ,$$

where crystalline orbitals of the *N*-electron system are expanded as linear combinations of a set of *m* Bloch functions built from *local atom-centered Gaussian-type functions* (GTFs):

$$\varphi_{\mathbf{k}i}(\mathbf{r}) = N \sum_{j=1}^{m} a_{ij}(\mathbf{k}) \left(\sum_{\mathbf{g}} \chi_{\mathbf{g}j}(\mathbf{r}) \exp(\mathrm{i}\mathbf{k} \cdot \mathbf{g}) \right) \ ,$$

where **k** is the wave vector of the irreducible representation of the group of crystal translations {**g**}. Atomic Gaussian-type functions $\chi_{\mathbf{g}j}(\mathbf{r})$ are defined as:

$$\chi_{\mathbf{g}j}(\mathbf{r} - \mathbf{A}_j) = \sum_{\mu}^{n_G} c_\mu G(\alpha_\mu; \mathbf{r} - \mathbf{A}_j - \mathbf{g}) \ ,$$

where $\mathbf{A}_j$ denotes the coordinate of nucleus in the zero cell of which atomic function $\chi_{\mathbf{g}j}(\mathbf{r})$ is centered; ***G***, $\boldsymbol{c}_\mu$ and α_μ are normalized GTF, its coefficients and exponents, respectively.

4. *CRYSTAL* calculations: HF, DFT and hybrid hamiltonians

Crystalline Hamiltonian is constructed using either HF or DFT formalisms using either *direct* or *reciprocal* spaces:

$$\hat{H}^{HF} = \hat{T}(\mathbf{r};\mathbf{k}) + \hat{V}(\mathbf{r};\mathbf{k}) + \hat{J}(\mathbf{r};\mathbf{k}) + \hat{K}(\mathbf{r};\mathbf{k})$$

$$\hat{H}^{KS} = \hat{T}(\mathbf{r};\mathbf{k}) + \hat{V}(\mathbf{r};\mathbf{k}) + \hat{J}\left[\rho(\mathbf{r});\mathbf{k}\right] + \hat{v}_{xc}\left[\rho(\mathbf{r});\mathbf{k}\right],$$

where $\hat{T}$, $\hat{V}$, $\hat{J}$ and $\hat{K}$ are *kinetic, electron-nuclei, Coulomb and exchange* operators, $\rho(\mathbf{r})$ *electron density function*, $\hat{v}_{xc}$ *exchange-correlation operator* depending on *xc*-functional:

$$\hat{v}_{xc} = \frac{\partial E_{xc}\left[\rho(\mathbf{r});\mathbf{k}\right]}{\partial \rho(\mathbf{r})},$$

CRYSTAL-09 code realizes partial incorporation of the exact non-local HF exchange into the non-local DFT exchange functional, with varying mixing *ratio*. There can be used **hybrid** *B3LYP, B3PW and PBE0* exchange-correlation energy functionals :

$$E_{xc}^{B3LYP} = (1-a_h)(E_x^{LDA} + a_x E_x^{Becke}) + a_h E_x^{HF} + (1-a_c)E_c^{GGA} + a_c E_c^{LYP}$$

$$E_{xc}^{B3PW} = (1-a_h)E_x^{LDA} + a_x E_x^{Becke} + a_h E_x^{HF} + a_c E_c^{PWGGA},$$

$$E_{xc}^{PBE0} = E_{xc}^{GGA} + a_x (E_x^{HF} + E_x^{GGA})$$

where a_h is input parameter of the HF/DFT exchange mixing; a_x and a_c are input parameters of the DFT exchange (*x*) and correlation (*c*) non-locality (*GGA/LDA*), respectively;

2. *CRYSTAL* calculations: HF, DFT and hybrid hamiltonians

a) Total energy calculation of the only configuration of periodic system[1]

Geometry and basis set input; symmetry analysis; integrals classification; computation of mono- and bi-electronic integrals

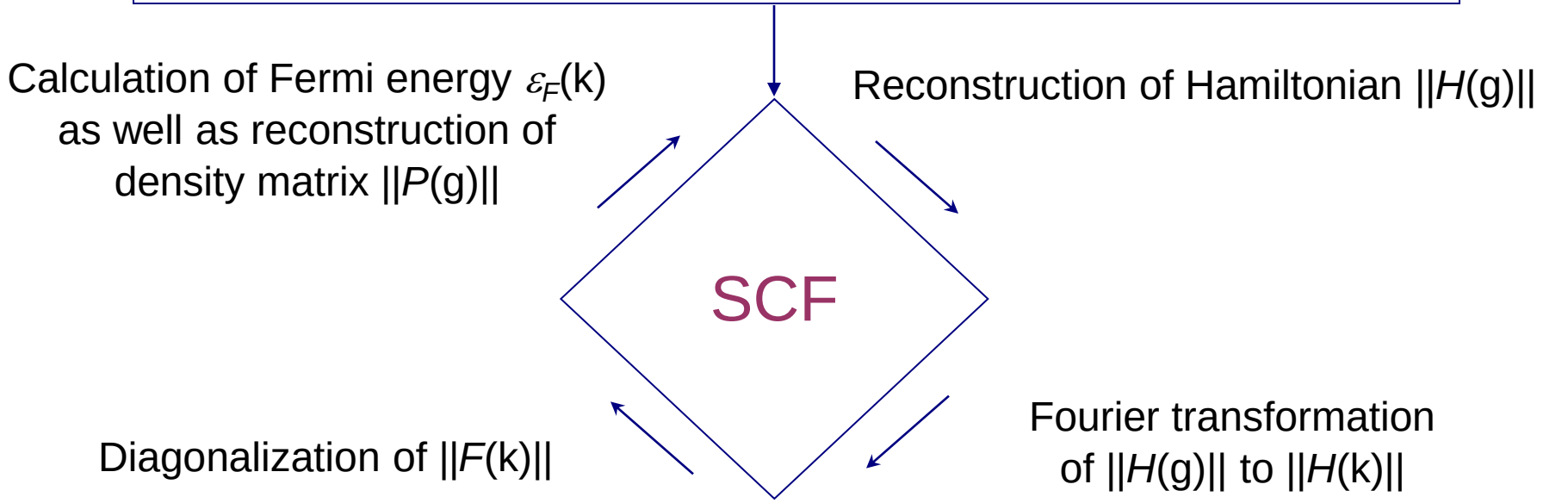

The SCF is completed after *n*-th iteration, when either tolerance of the total energy *per* unit cell (UC) is achieved, or *n* cycles exceeds limit of iterations.

b) Geometry optimization of system with successive total energy re-calculation[1]

A modified conjugate gradient algorithm is used to optimize the atomic coordinates and to locate minima on the potential energy surface

[1] Dovesi, R.; Saunders, V. R.; Roetti, C.; Orlando, R.; Zicovich-Wilson, C. M.; Pascale, F.; Civalleri, B.; Doll, K.; Harrison, N. M.; Bush, I. J.; D'Arco, Ph.; Llunell, M. *CRYSTAL-2009* User Manual: University of Turin: Turin 2009.

3. Models and properties of perfect BN, TiO_2 and $SrTiO_3$ SW NTs

3. Models and properties of BN and TiO_2 SW NTs

J. Phys. Chem. C **2010,** *114,* 21061–21069

Symmetry and Models of Single-Wall BN and TiO_2 Nanotubes with Hexagonal Morphology

R. A. Evarestov,*,† Yu. F. Zhukovskii,‡ A. V. Bandura,† and S. Piskunov‡,§,∥

Department of Quantum Chemistry, St. Petersburg State University, 26 Universitetsky Avenue, Petrodvorets 198504, Russia, Institute of Solid State Physics, University of Latvia, 8 Kengaraga Str., Riga LV-1063 Latvia, Faculty of Computing, University of Latvia, 19 Raina Blvd., Riga LV-1586, Latvia, and Faculty of Physics and Mathematics, University of Latvia, 8 Zellu Str., Riga LV-1002, Latvia

Cent. Eur. J. Phys. • 9(2) • 2011 • 492-501
DOI: 10.2478/s11534-010-0095-8

VERSITA

Central European Journal of **Physics**

Symmetry and models of single-walled TiO_2 nanotubes with rectangular morphology*

Research Article

Robert A. Evarestov[1†], Yuri F. Zhukovskii[2], Andrei V. Bandura[1], Sergei Piskunov[2,3,4]

1 *Department of Quantum Chemistry, St. Petersburg State University, 26 Universitetsky Avenue, Petrodvorets 198504, Russia*

2 *Institute of Solid State Physics, University of Latvia, 8 Kengaraga Str., Riga LV-1063 Latvia*

3 *Faculty of Computing, University of Latvia, 19 Raina Blvd., Riga LV-1586, Latvia*

4 *Faculty of Physics and Mathematics, University of Latvia, 8 Zellu Str., Riga LV-1002, Latvia*

3a. BN SW NANOTUBES

Models of BN sheet&nanotubes

Monolayer BN(001) sheet: atop&across images

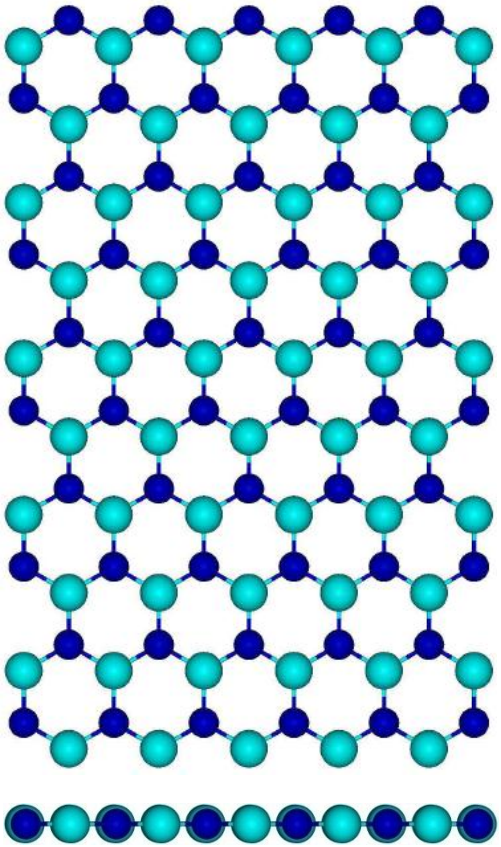

optimized single-wall (6,6) BN NT (aside&across images), D_{NT} = 0.84 nm

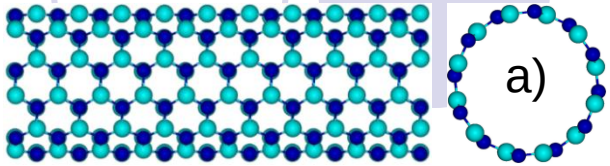

optimized single-wall (12,0) BN NT (aside&across images), D_{NT} = 0.96 nm

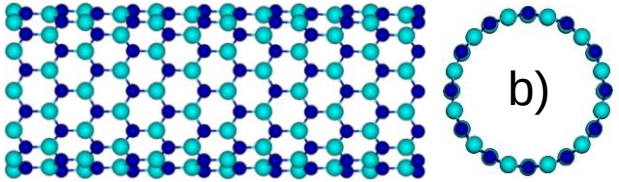

optimized single-wall (18,18) BN NT (aside&across images), D_{NT} = 2.49 nm

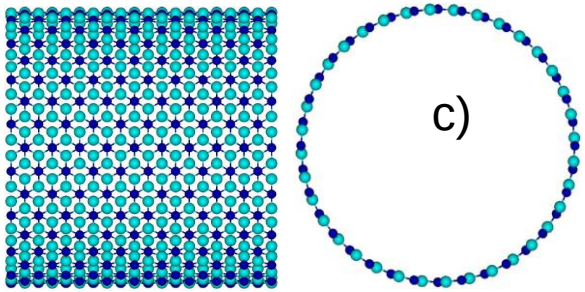

optimized single-wall (36,0) BN NT (aside&across images), D_{NT} = 2.87 nm

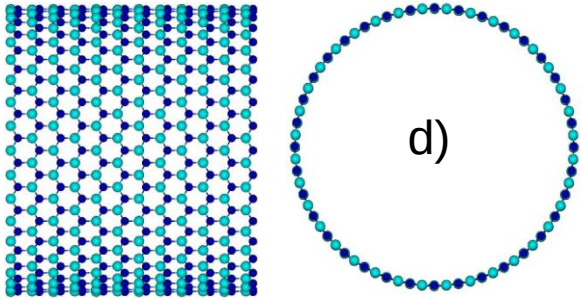

Yu.F. Zhukovskii, S. Piskunov, N. Pugno, B. Berzina, L. Trinkler, S. Bellucci, J. Phys. Chem. Solids, 70, 796-803 (2009).

3b. TiO_2 SW NANOTUBES

Models of stoichiometric titania sheets of different thickness optimized from the corresponding slabs with initial geometry of bulk anatase (atop&across images)

a) 3-layer fluorite-type TiO_2 (111) slab, (thickness 0.19 nm)

b) 6-layer anatase-type TiO_2 (101) slab (thickness 0.24 nm)

c) 12-layer anatase-type TiO_2 (101) slab (thickness 0.58 nm)

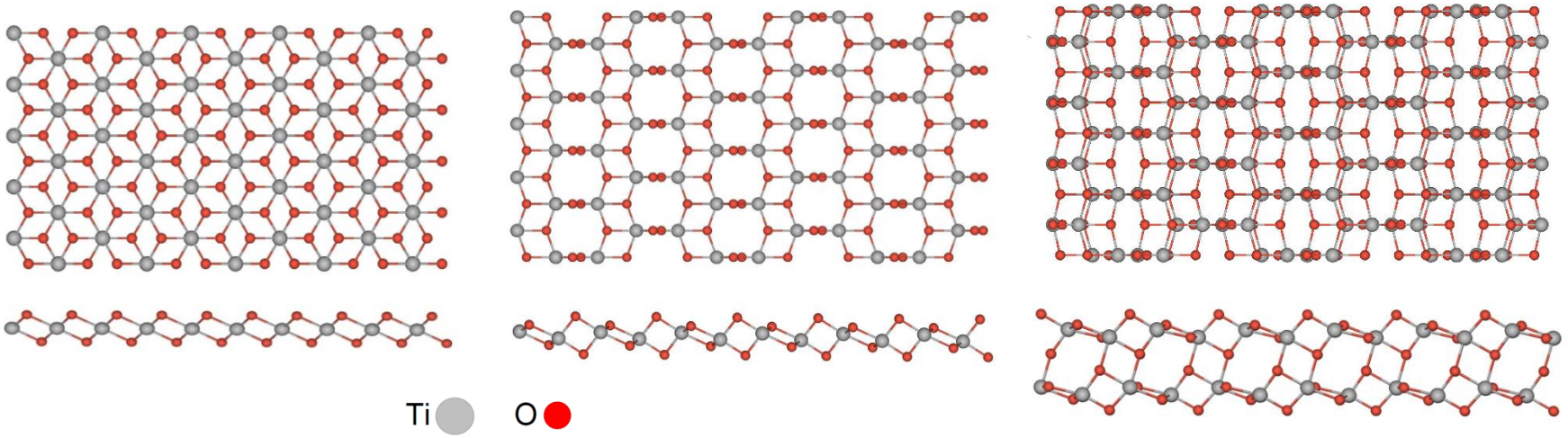

When optimizing geometry of 3-layer slab, we have observed spontaneous (barrier-less) phase transition from anatase to fluorite phase. Optimization of 6- and 12-layer sheets results in lattice compression along horizontal direction (according to slide oprientaition) as compared to bulk phase. Thus, properties of 3-layer sheets differ from those obtained for 6- and 12-layer anatase slabs.

3b. TiO_2 SW NANOTUBES

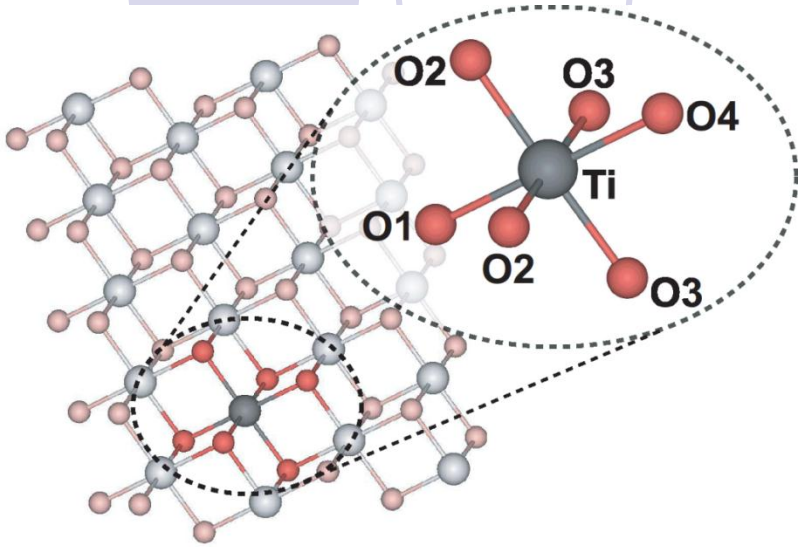

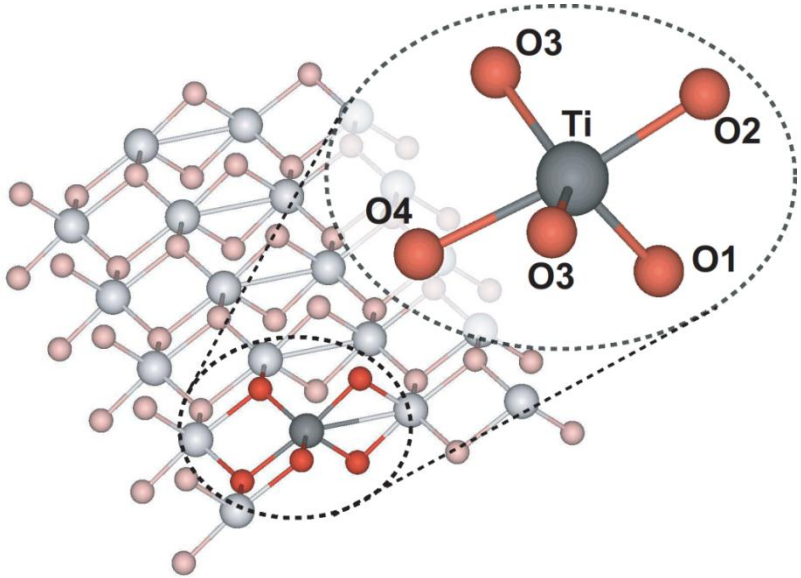

Two different types of coordination for Ti atoms in:

(a) three-layer hexagonal titania sheets (six-fold)

(b) six-layer centered rectangular titania sheets (five-fold).

3b. TiO_2 SW NANOTUBES

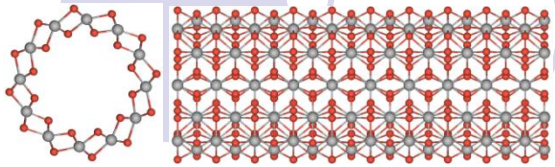

a) SW (6,6) nanotube (across&aside images and DOS), D_{NT} = 1.01 nm

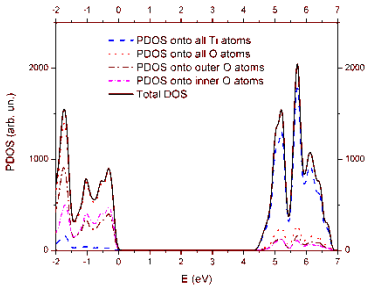

Optimized 3-layer fluorite-type TiO_2 NTs

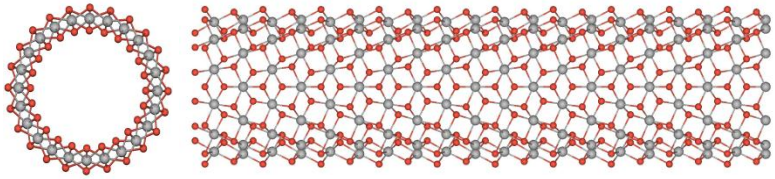

b) SW (12,0) nanotube (across&aside images and DOS), D_{NT} = 1.17 nm

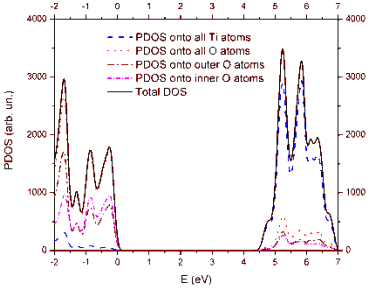

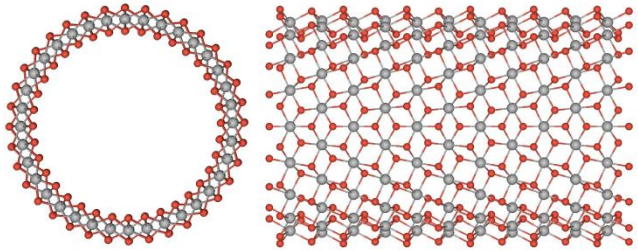

c) SW (18,0) nanotube (across&aside images and DOS), D_{NT} = 1.72 nm

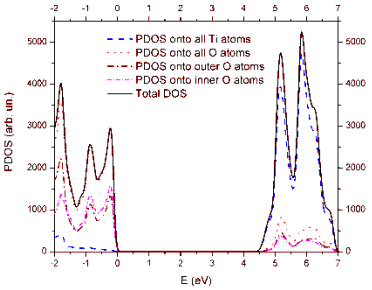

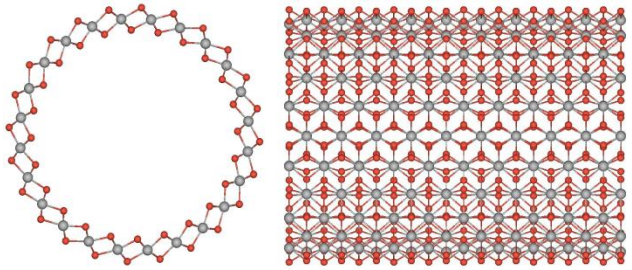

d) SW (12,12) nanotube (across&aside images and DOS), D_{NT} = 1.97 nm

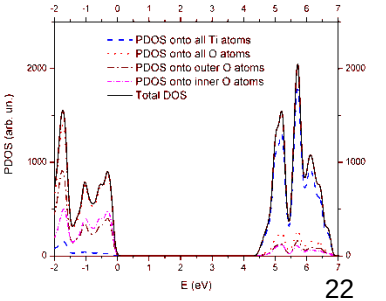

3b. TiO_2 SW NANOTUBES

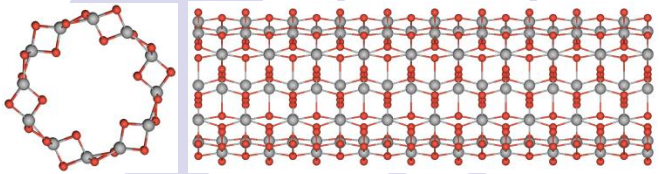

a) SW (-3,3) nanotube (across&aside images and DOS), D_{NT} = 1.00 nm

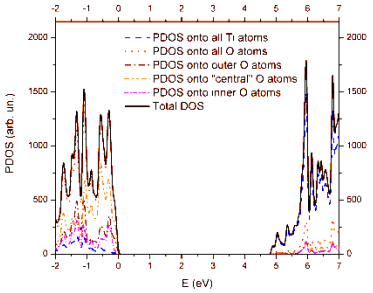

Optimized 6-layer anatase-type TiO_2 NTs

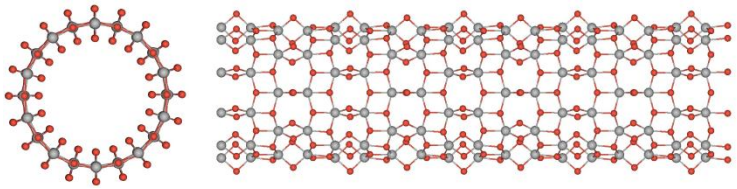

b) SW (10,10) nanotube (across&aside images and DOS), D_{NT} = 1.18 nm

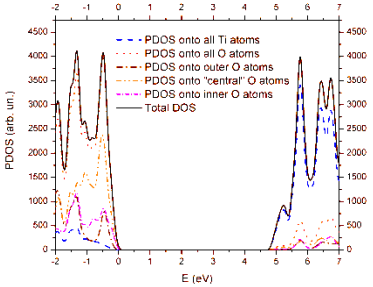

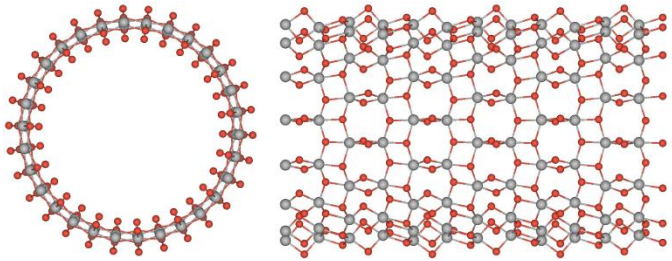

c) SW (15,15) nanotube (across&aside images and DOS), D_{NT} = 1.73 nm

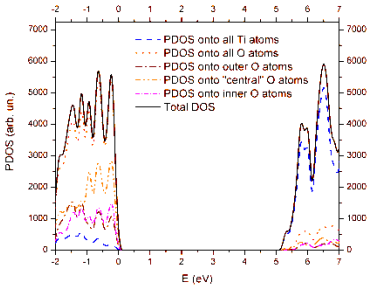

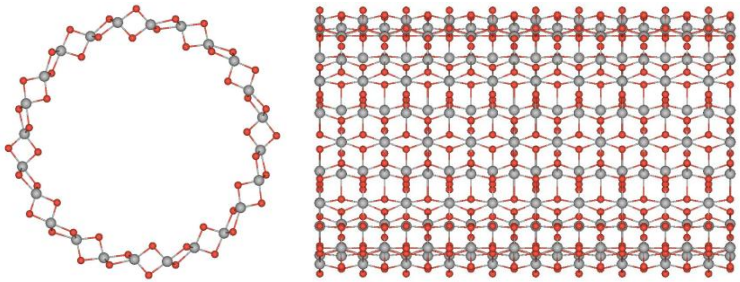

d) SW (-6,6) TiO_2 NT (across&aside images and DOS), D_{NT} = 1.98 nm

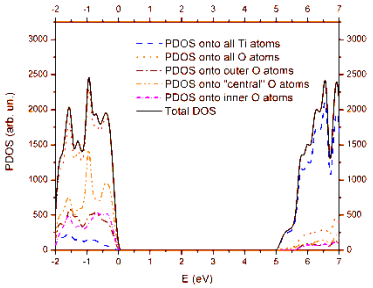

A.V. Bandura, R.A. Evarestov, *Surf. Sci.* 603, L117-L120 (2009) .

3a&b. BN *vs.* HEXAGONAL TiO_2 SW NANOTUBES

The strain energy (E_{strain}) *vs.* nanotube diameter (D_{NT}) for two pairs of sets for SW BN NTs and 3-layer SW TiO_2 NTs, both with *hexagonal* (*n*,*n*) and (*n*,*0*) chiralities

There exist much more qualitative similarities between the $E_{strain}(D_{NT})$ curves for hexagonal nanotubes of different chemical nature than between those for NTs of different phases of the same titania.

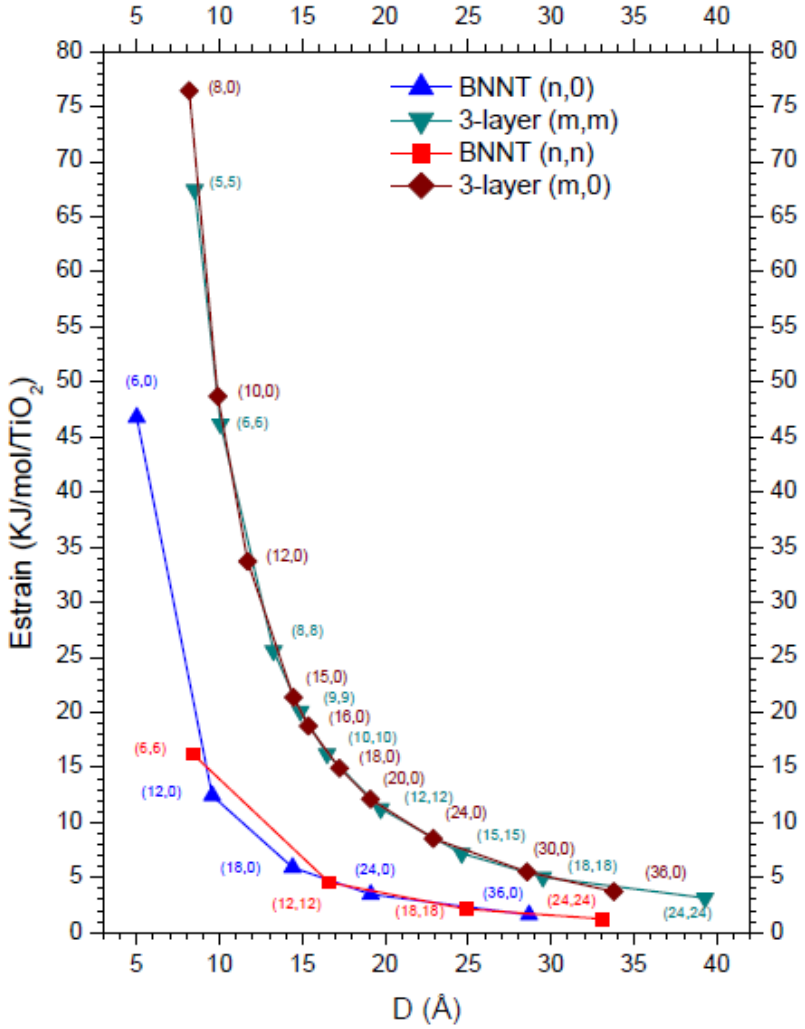

3a&b. BN *vs.* HEXAGONAL TiO_2 NANOTUBES

The band gap ($\Delta\varepsilon_{gap}$) *vs.* nanotube diameter (D_{NT}) for two pairs of sets for SW BN NTs and 3-layer SW TiO_2 NTs, both with *hexagonal* (*n*,*n*) and (*n*,*0*) chiralities

There exist much more qualitative similarities between the $\Delta\varepsilon_{gap}(D_{NT})$ curves for hexagonal nanotubes of different chemical nature than between those for NTs of different phases of the same titania.

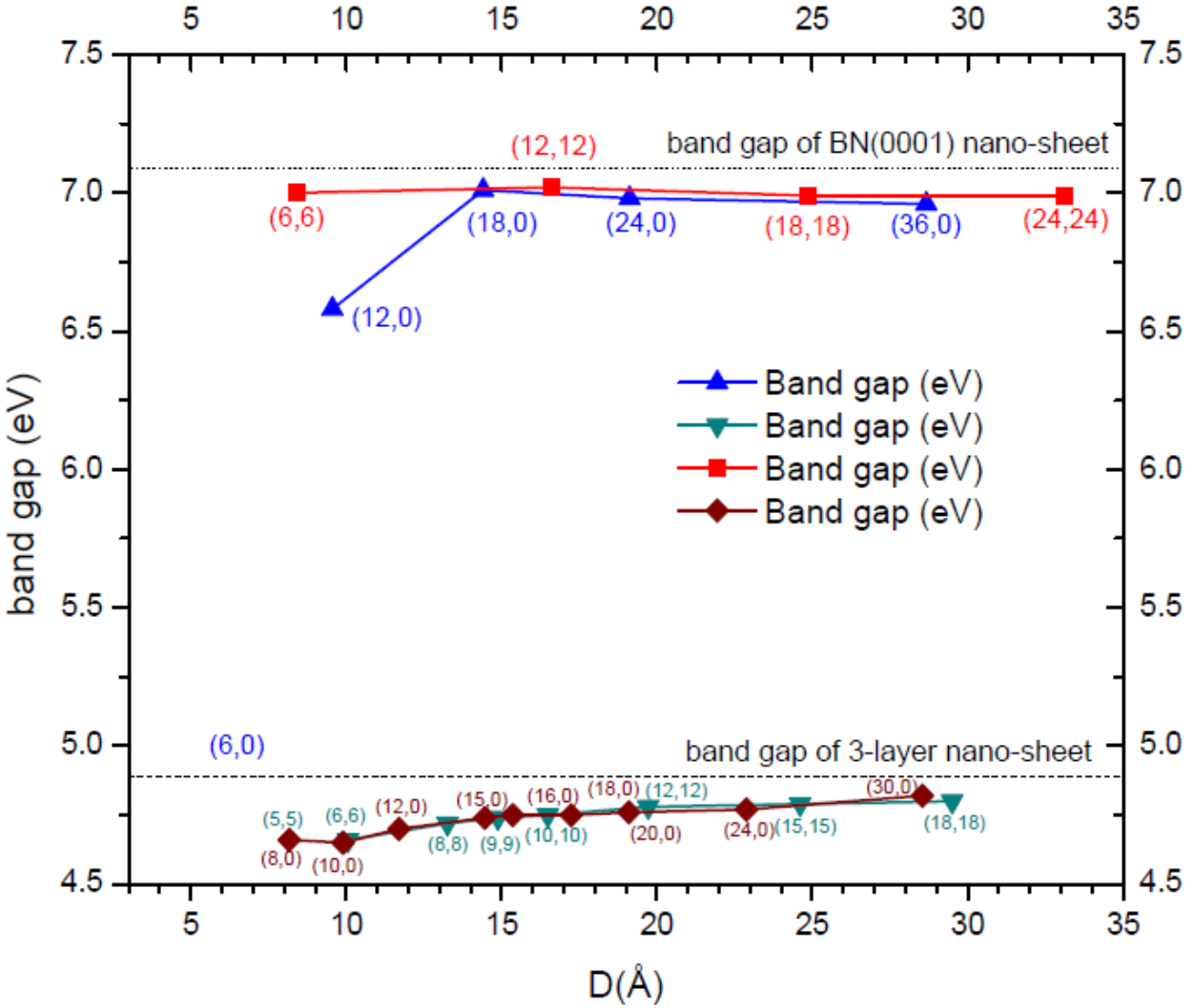

3c. Models and properties of $SrTiO_2$ SW NTs

THE JOURNAL OF PHYSICAL CHEMISTRY Letters

LETTER

pubs.acs.org/JPCL

$SrTiO_3$ Nanotubes with Negative Strain Energy Predicted from First Principles

Sergei Piskunov*,† and Eckhard Spohr‡

†Faculty of Computing, University of Latvia, 19 Raina Blvd., Riga LV-1586, Latvia, Faculty of Physics and Mathematics, University of Latvia, 8 Zellu Str., Riga LV-1002, Latvia, and Institute for Solid State Physics, University of Latvia, 8 Kengaraga Str., Riga LV-1063, Latvia

‡Department of Theoretical Chemistry, University of Duisburg-Essen, Universitätstr. 2, D-45141 Essen, Germany

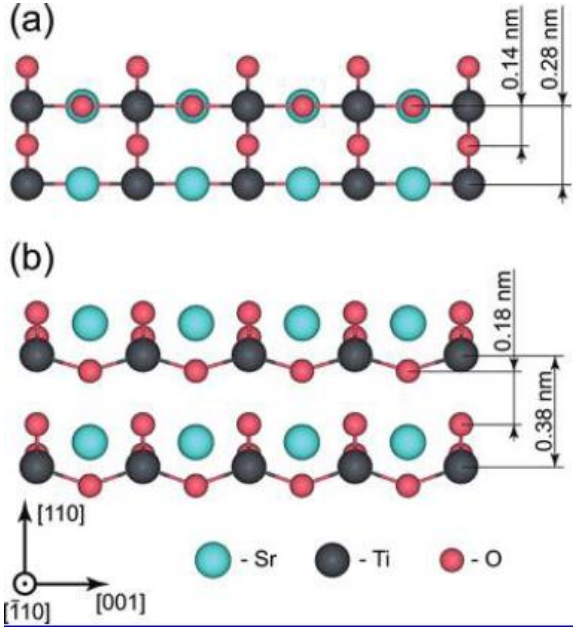

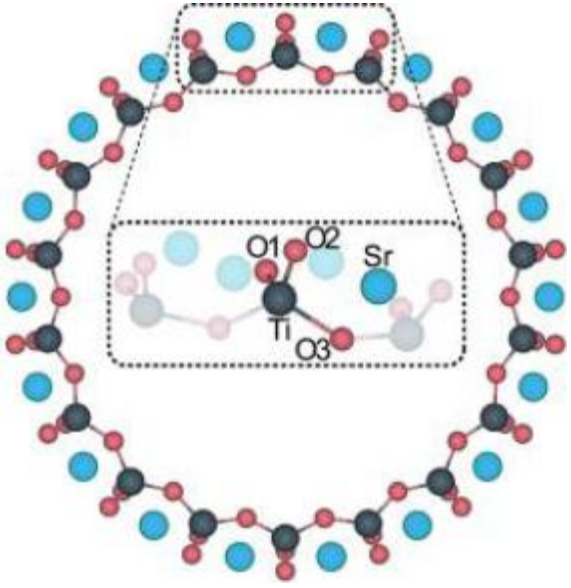

3c. Models and properties of $SrTiO_2$ SW NTs

The strain energy (E_{strain}) *vs.* nanotube diameter (D_{NT}) for two structural types of $SrTiO_3$ nanotubes with different chiralities

On the basis of hybrid density functional theory calculations, we predict that the most energetically favorable single-walled $SrTiO_3$ nanotubes with negative strain energy can be folded from $SrTiO_3$ (110) nanosheets of rectangular morphology. Further formation of multi-walled tubular nanostructure with inter-wall distance of~0.46 nm yields an additional gain in energy of 0.013 eV per formula unit. (The formation energy of the most stable nanotube is 1.36 eV/$SrTiO_3$.) Because of increase in the TiO bond covalency in the outer shells, $SrTiO_3$ nanotubes can demonstrate an enhancement of their adsorption properties. Quantum confinement leads to a widening of the energy band gap of single-walled $SrTiO_3$ nanotubes (~6.1 eV) relative to the bulk (~3.6 eV), which makes them attractive for further band gap engineering.

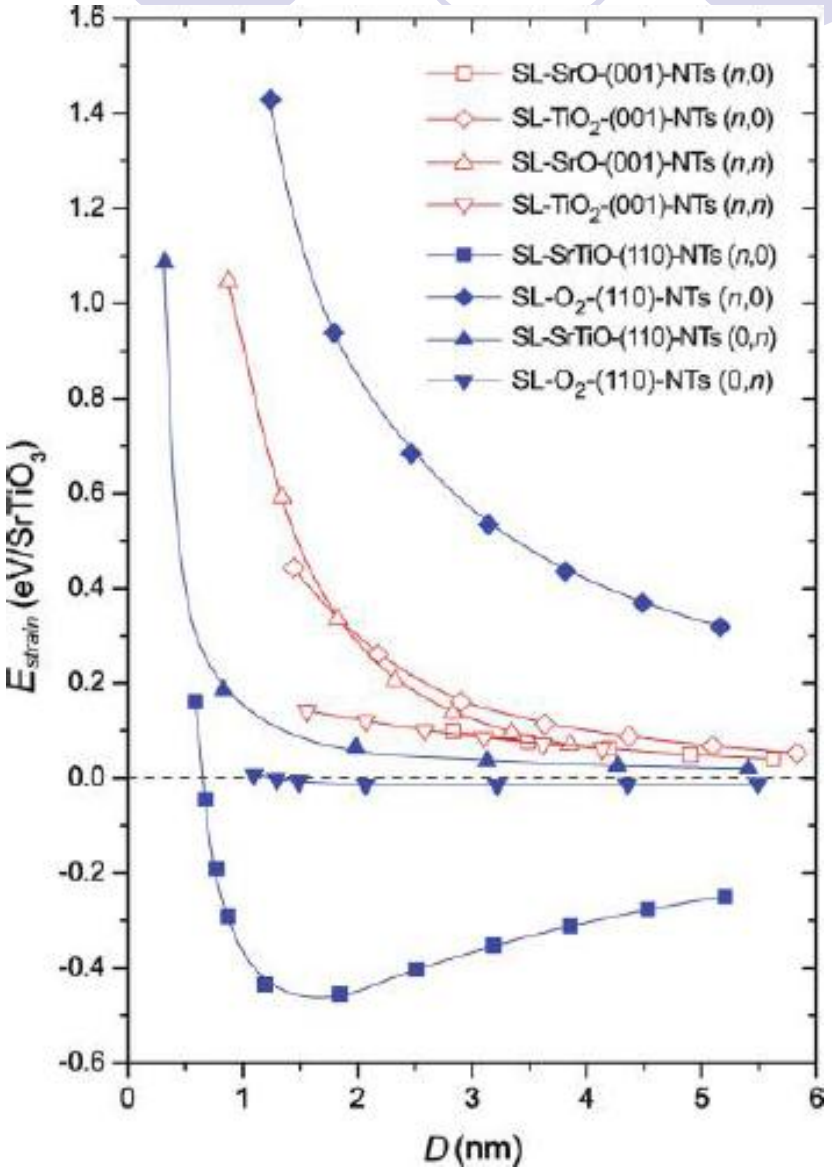

3. Summary and predictions

1. We have elaborated simulation formalism for theoretical modeling of inrganic nanotubes based on large-scale DFT-LCAO calculations on different structural and electronic properties of perfect and defective perfect BN, TiO_2 and $SrTiO_3$ nanotubes of different chiralities and diameters. The strain energies of single-wall BN nanotubes are considerably smaller than those for both aforementioned types of single-wall TiO_2 NTs, thus being more stable energetically. This formalism can be applied for other types of inorganic nanotubes. For the first time, we have described TiO_2 and $SrTiO_3$ nanotubes with negative strained energies which means their spontaneous formation from metatable 2D nanosheets..

2. Use of the line group formalism allows the construction of nanotubes of different crystalline morphology. The exploitation of the rotohelical symmetry of NTs, usually quite high, permits to drastically reduce the computation time.

3. *Ab initio LCAO* calculations using the hybrid *PBE0* Hamiltonian allow us to perform the analysis of the atomic and electronic structure of BN and TiO_2 slabs, nanotubes simulated using different models.

4. Models and properties of perfect BN and TiO_2 DW NTs

4. Models and properties of DW BN and TiO_2 NTs

THE JOURNAL OF PHYSICAL CHEMISTRY C

ARTICLE

pubs.acs.org/JPCC

J. Phys. Chem. C 2011, 115, 14067–14076

Symmetry and Models of Double-Wall BN and TiO_2 Nanotubes with Hexagonal Morphology

R. A. Evarestov,[*,†] Yu. F. Zhukovskii,[‡] A. V. Bandura,[†] S. Piskunov,[‡,§,∥] and M. V. Losev[†]

[†]Department of Quantum Chemistry, St. Petersburg State University, 26 Universitetsky Avenue, Petrodvorets 198504, Russia

[‡]Institute of Solid State Physics, University of Latvia, 8 Kengaraga Street, Riga LV-1063, Latvia

[§]Faculty of Computing, University of Latvia, 19 Raina Boulevard, Riga LV-1586, Latvia

[∥]Faculty of Physics and Mathematics, University of Latvia, 8 Zellu Street, Riga LV-1002, Latvia

Annual Conference on Functional Materials and Nanotechnologies – FM&NT 2011 IOP Publishing

IOP Conf. Series: Materials Science and Engineering **23** (2011) 012014 doi:10.1088/1757-899X/23/1/012014

First-principles calculations on double-walled inorganic nanotubes with hexagonal chiralities

Yuri F Zhukovskii[*1], Robert A Evarestov[2], Andrei V Bandura[2], Maxim V Losev[2]

[1]Institute of Solid State Physics, University of Latvia, 8 Kengaraga Str., LV-1063, Riga, Latvia.

[2]Department of Quantum Chemistry, St. Petersburg State University, 26 Universitetsky Ave., 198504, Petrodvorets, Russia.

4a. Models and properties of DW BN NTs

a) model of straight double-wall (5,5)@(10,10) *ac*-BN NT;

b) model of straight (B-B) double-wall (9,0)@(18,0) *zz*-BN NT;

c) model of inversed (N-B) double-wall (9,0)@(18,0) *zz*-BN NT.

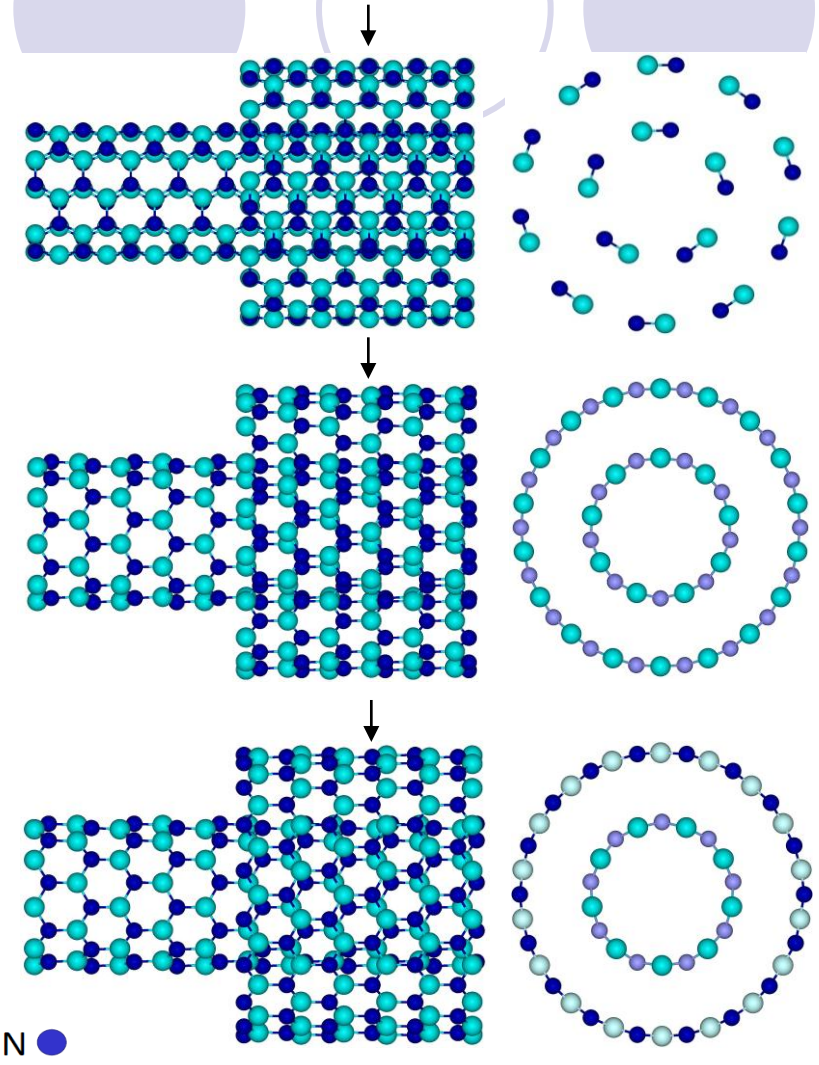

4a. Models and properties of DW BN NTs

The binding energy E_{bind} between the constituent shells of double-wall nanotube has been chosen as a criterion of nanotube stability:

$$-E_{bind}(D_{NT}^{in}@D_{NT}^{out}) = E_{tot}(D_{NT}^{in}@D_{NT}^{out}) - E_{tot}(D_{NT}^{in}) - E_{tot}(D_{NT}^{out}),$$

where E_{tot} are the calculated total energies of DW NT and its constituent SW NTs with optimized structure.

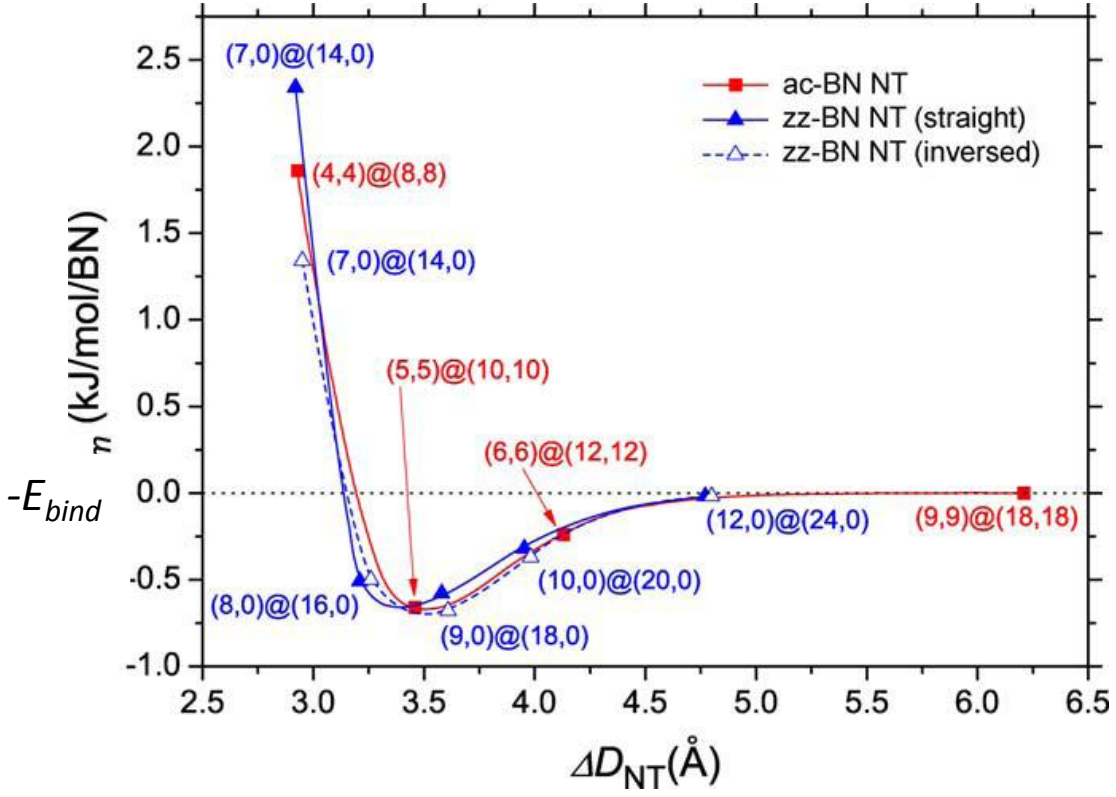

Binding energies E_{bind} *vs.* ΔD_{NT} for the three sets of DW BN NTs with *ac*- and *zz*-chiralities. Spline treatment of curves has been performed to make them smooth

4a. Models and properties of DW BN NTs

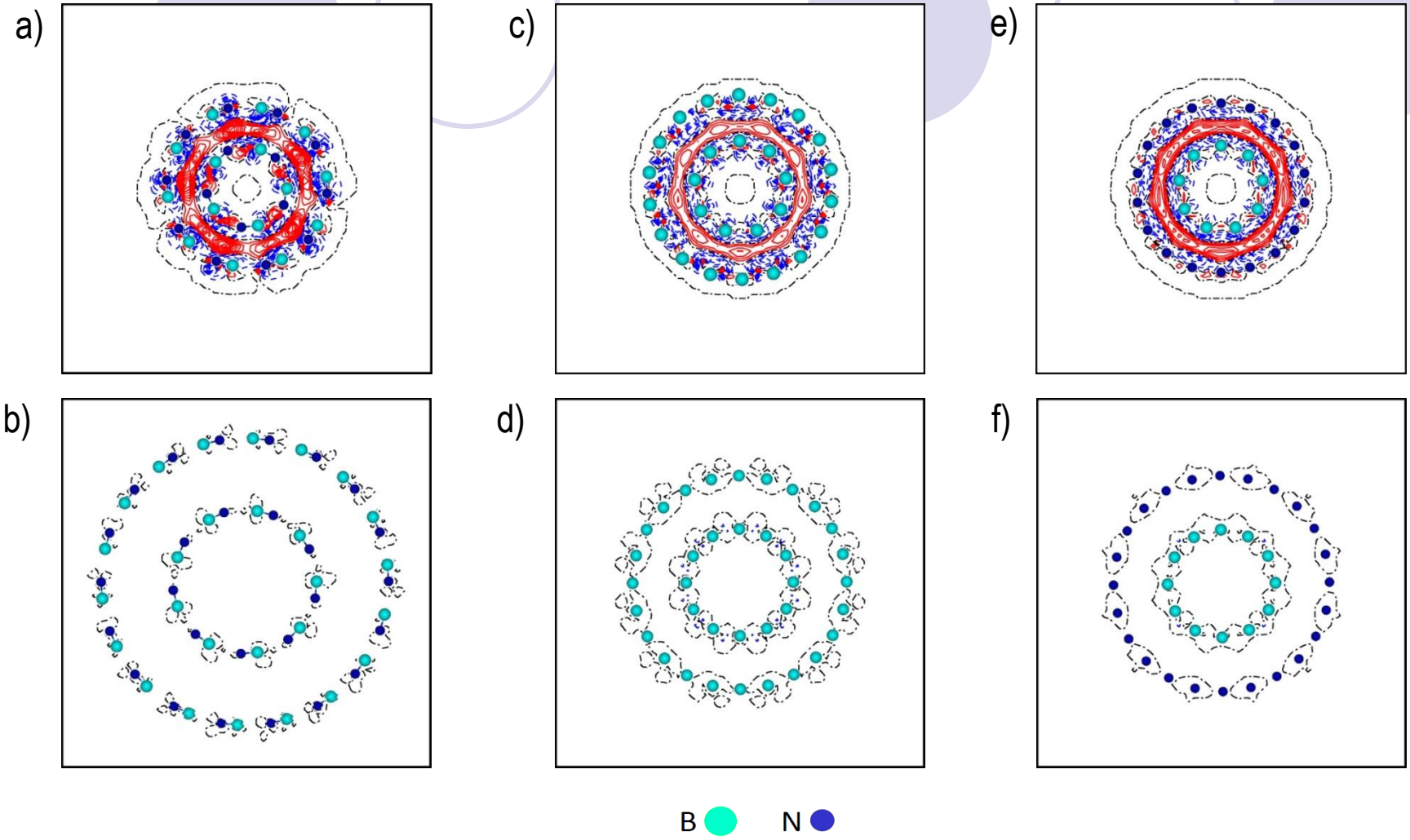

Difference electron density plots $\Delta\rho(\mathbf{r})$ (the total electron densities in the perfect DW BN NT minus the sum of these densities in the two constituent SW BN NTs) projected onto the section planes across NTs: a) (5,5)@(10,10), b) (9,9)@(18,18), c) straight (9,0)@(18,0), d) straight (12,0)@(24,0), e) inversed (9,0)@(18,0), f) inversed (12,0)@(24,0).

4b. Models and properties of DW TiO_2 NTs

a) optimized model of double-wall (6,6)@(12,12) *ac*-TiO_2 NT;

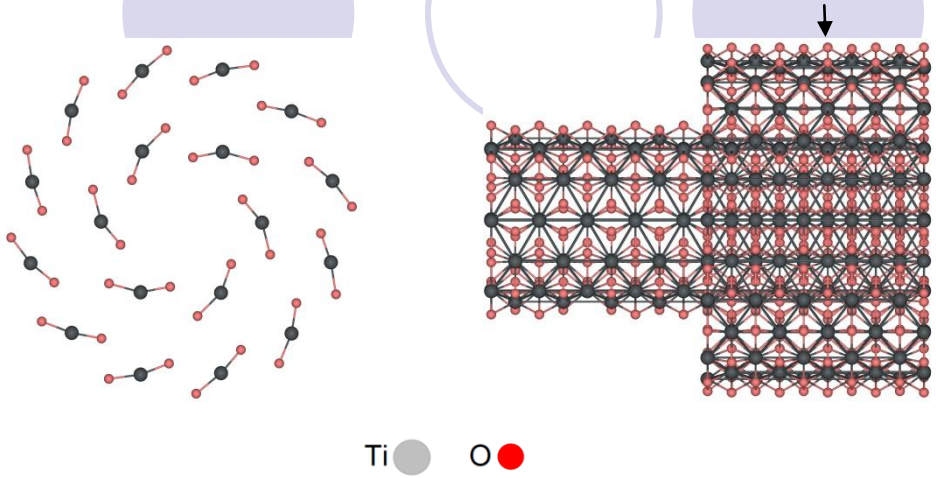

b) optimized model of double-wall (10,0)@(20,0) *zz*- TiO_2 NT.

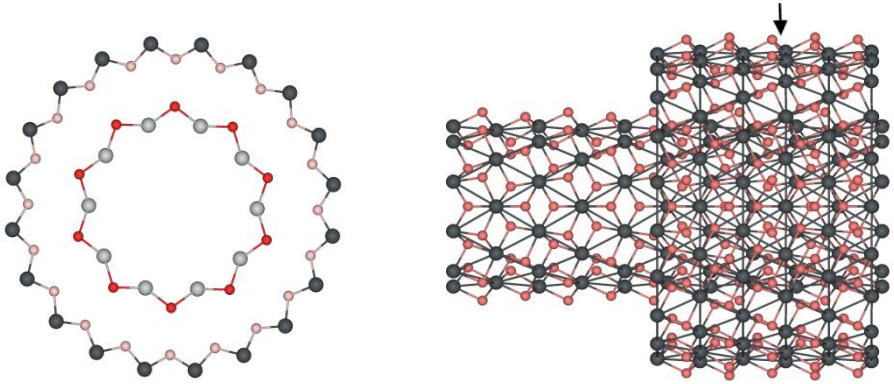

Cross-sections and aside images of hexagonal DW TiO_2 NTs corresponding to optimized diameters (*i.e.*, left and right parts of models a) and b), respectively) for armchair and zigzag chiralities. For *zz*-DW NT (b), there are also shown atoms of the nearest ring behind the cross-section (as considerably more light circles).

4b. Models and properties of DW TiO_2 NTs

The binding energy E_{bind} between the constituent shells of double-wall nanotube has been chosen as a criterion of nanotube stability:

$$-E_{bind}(D_{NT}^{in}@D_{NT}^{out}) = E_{tot}(D_{NT}^{in}@D_{NT}^{out}) - E_{tot}(D_{NT}^{in}) - E_{tot}(D_{NT}^{out}),$$

where E_{tot} are the calculated total energies of DW NT and its constituent SW NTs with optimized structure.

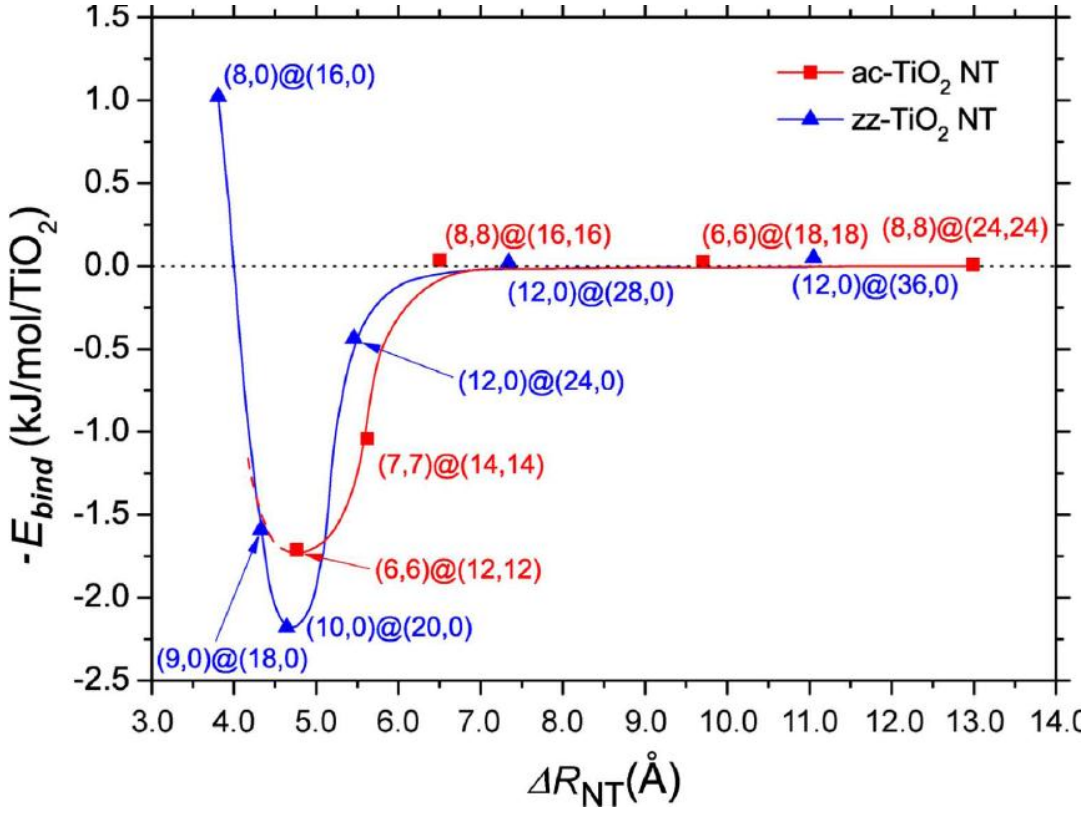

Binding energies E_{bind} *vs.* ΔD_{NT} for the three sets of DW TiO_2 NTs with *ac*- and *zz*-chiralities. Spline treatment of curves has been performed to make them smooth

4b. Models and properties of DW TiO_2 NTs

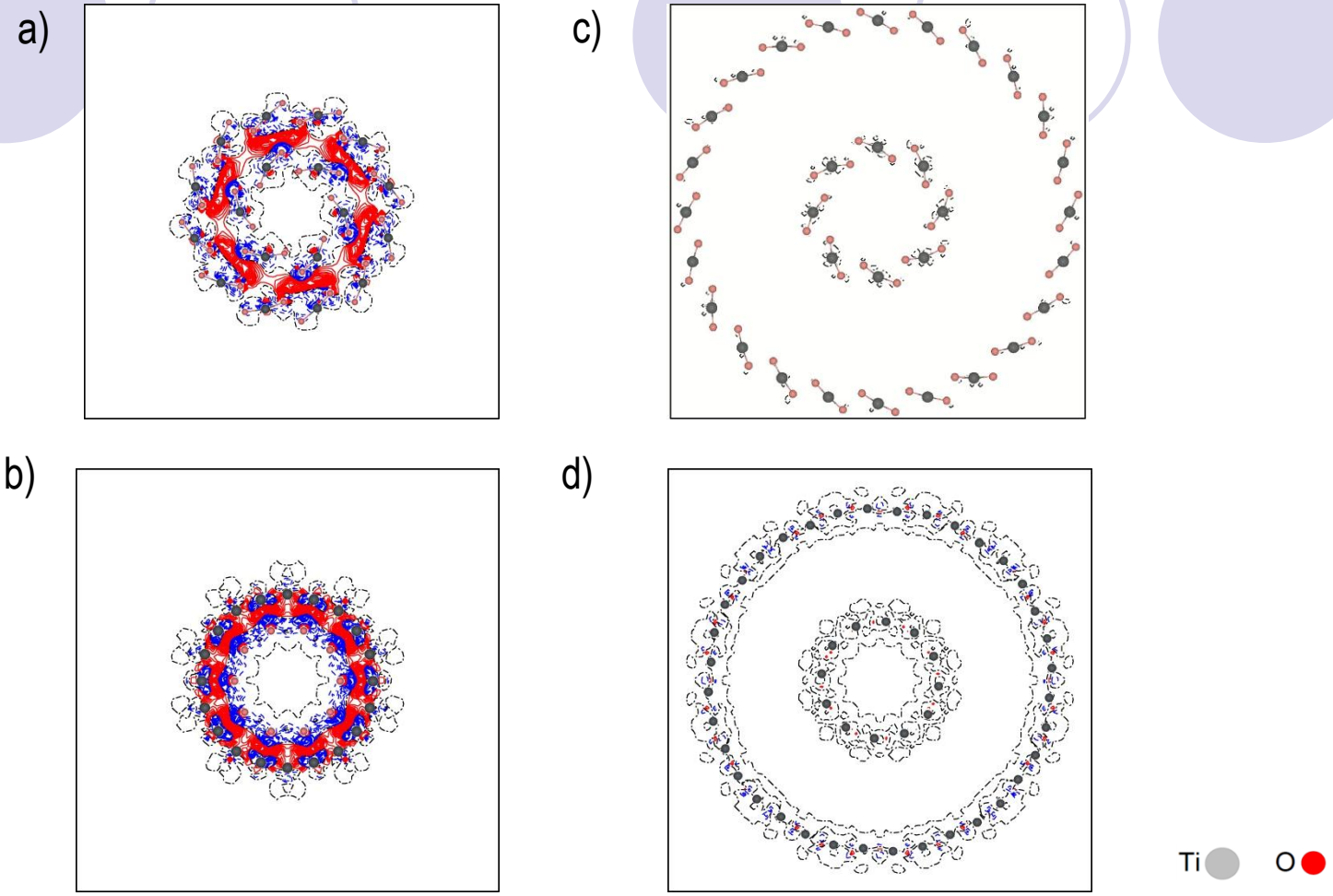

Difference electron density plots $\Delta\rho(\mathbf{r})$ (the total electron densities in the perfect DW TiO_2 NT minus the sum of these densities in the two constituent SW TiO_2 NTs) projected onto the section planes across NTs: a) (6,6)@(12,12), b) (8,8)@(24,24), c) (10,0)@(20,0) , d) (12,0)@(36,0).

4. Summary and predictions

1. Large-scale first-principles LCAO calculations using the hybrid PBE0 Hamiltonian have been performed for the analysis of the atomic and electronic structure of double-wall BN and TiO_2 nanotubes simulated using different models for different morphology. To the best of our knowledge, calculations on DW TiO_2 NTs have been performed by us for the first time.

2. To estimate stability of DW BN and TiO_2 NTs, we have chosen the binding energies between their constituent shells (E_{bind}) as a criterion. These binding energies depend mainly on the inter-wall distance (ΔD_{NT}) and the diameter of the internal shell. The potential energy curves $E_{bind}(\Delta D_{NT})$ for double-wall nanotubes of both chiralities permit to estimate their equilibrium configurations: (5,5)@(10,10) and (9,0)@(18,0) chiralities for BN NTs as well as (6,6)@(11,11) and (10,0)@(20,0) for TiO_2 NTs. The values of ΔD_{NT} and , which are smaller than those in equilibrium configurations, lead to instability of DW NTs, while their large values correspond to quasi-independent non-interacting pairs of SW NTs.

3. The inversed structure of double-wall *zz*-BN NT has been found to be energetically more preferable than its straight configuration, due to additional electrostatic attraction of the closest positively and negatively charged nanotube rings and repulsion of analogous rings consisting of the same type of atoms. Obviously, results obtained for inversed configuration favor to the dipolar-shell structural morphology of MW BN NTs earlier observed experimentally.

4. Considerable interaction between the walls in equilibrium DW NT configurations results in a decrease of band gaps in double-wall nanotubes as compared to those for SW NTs (this decrease is a more pronounced for DW TiO_2 NTs).

5. Models and properties of defective BN, TiO_2 and $SrTiO_3$ SW NTs

5a. Models and properties of BN SW NTs with single defects

Eur. Phys. J. B **67**, 519–525 (2009)
DOI: 10.1140/epjb/e2009-00038-2

THE EUROPEAN PHYSICAL JOURNAL B

Regular Article

Atomic and electronic structure of single-walled BN nanotubes containing N vacancies as well as C and O substitutes of N atoms

Y.F. Zhukovskii[1,2], S. Bellucci[3,a], S. Piskunov[1,4], L. Trinkler[1], and B. Berzina[1]

[1] Institute of Solid State Physics, University of Latvia, Kengaraga Str. 8, 1063 Riga, Latvia
[2] Materials Research Center, Northwestern University, 2145 Sheridan Rd., 60208 Evanston IL, USA
[3] Laboratori Nazionali di Frascati, Istituto Nazionale di Fisica Nucleare, Via E. Fermi 40, 00044 Frascati (Rome), Italy
[4] Lehrstuhl für Theoretische Chemie, Universität Duisburg-Essen, Universitätsstr. 5, 45141 Essen, Germany

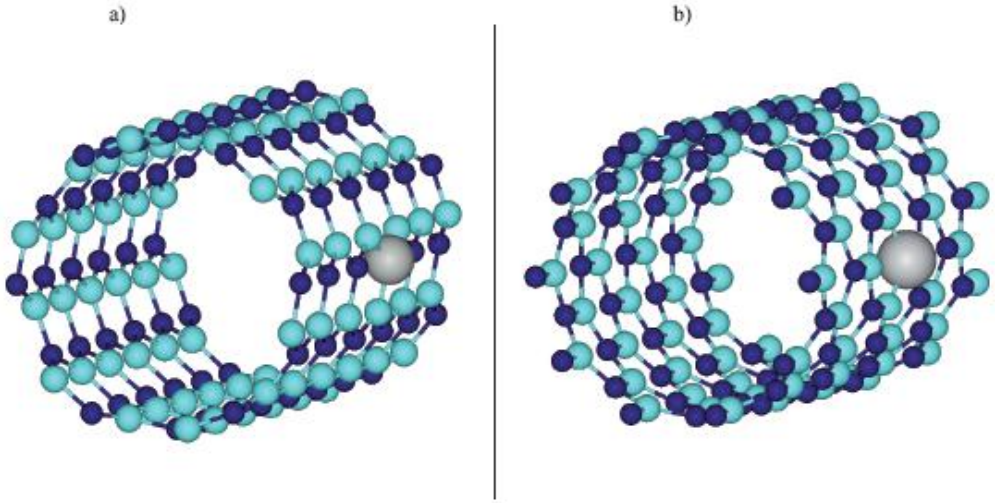

5a. Models and properties of BN SW NTs with single defects

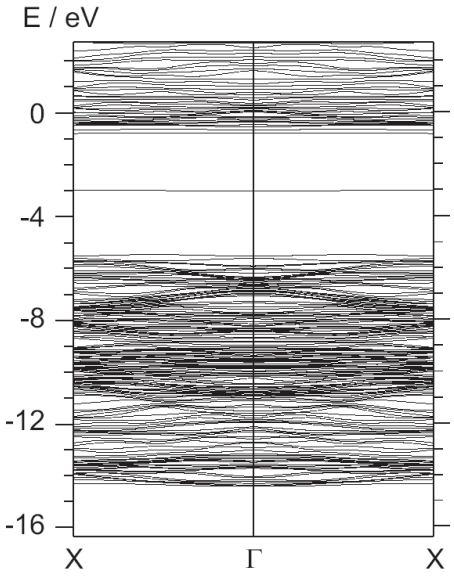

(a)

Band structures for 0.8 nm BN-*F* nanotubes with different values of $d_{F\text{-}F}$: *armchair*-type (8.4 and 16.2 Å, a,c) and *zigzag-type* NTs (10.8 and 17.3 Å b,d)

There is a twice-degenerated defect level induced by N vacancy inside the NT band gap: a_1 energy level, consisting of mainly B(*2s*) state partially hybridized with B(*2p*), which lies ~2.5 and ~2.1 eV above the top VB for armchair- and zigzag-type structure, respectively (second degenerated non-populated sublevel is locaeted 0.1-0.2 eV below the bottom of conductance band. Dispersion of defect levels presented in plots (for $d_{F\text{-}F} > 15$ Å in BN NTs of both chiralities) is neglecting (*i.e.*, lines of levels are practically straight.

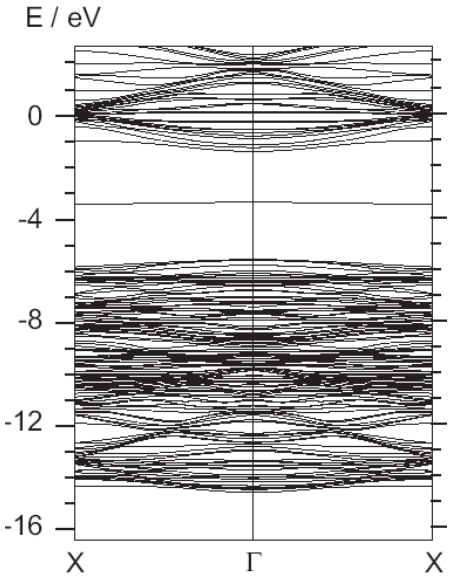

(b)

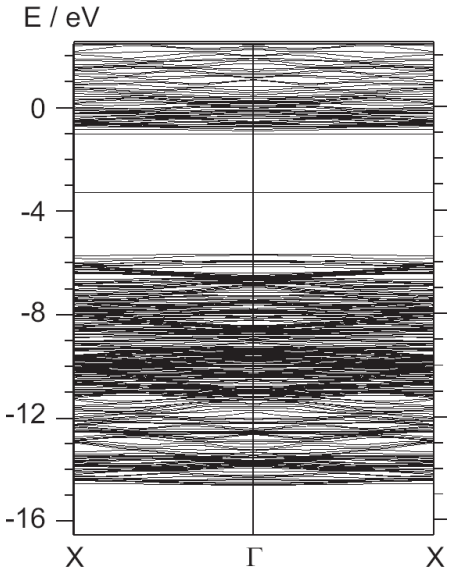

(c)

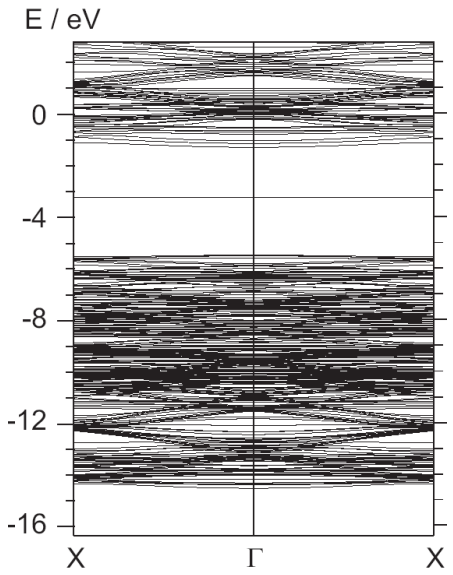

(d)

5a. Models and properties of BN SW NTs with single defects

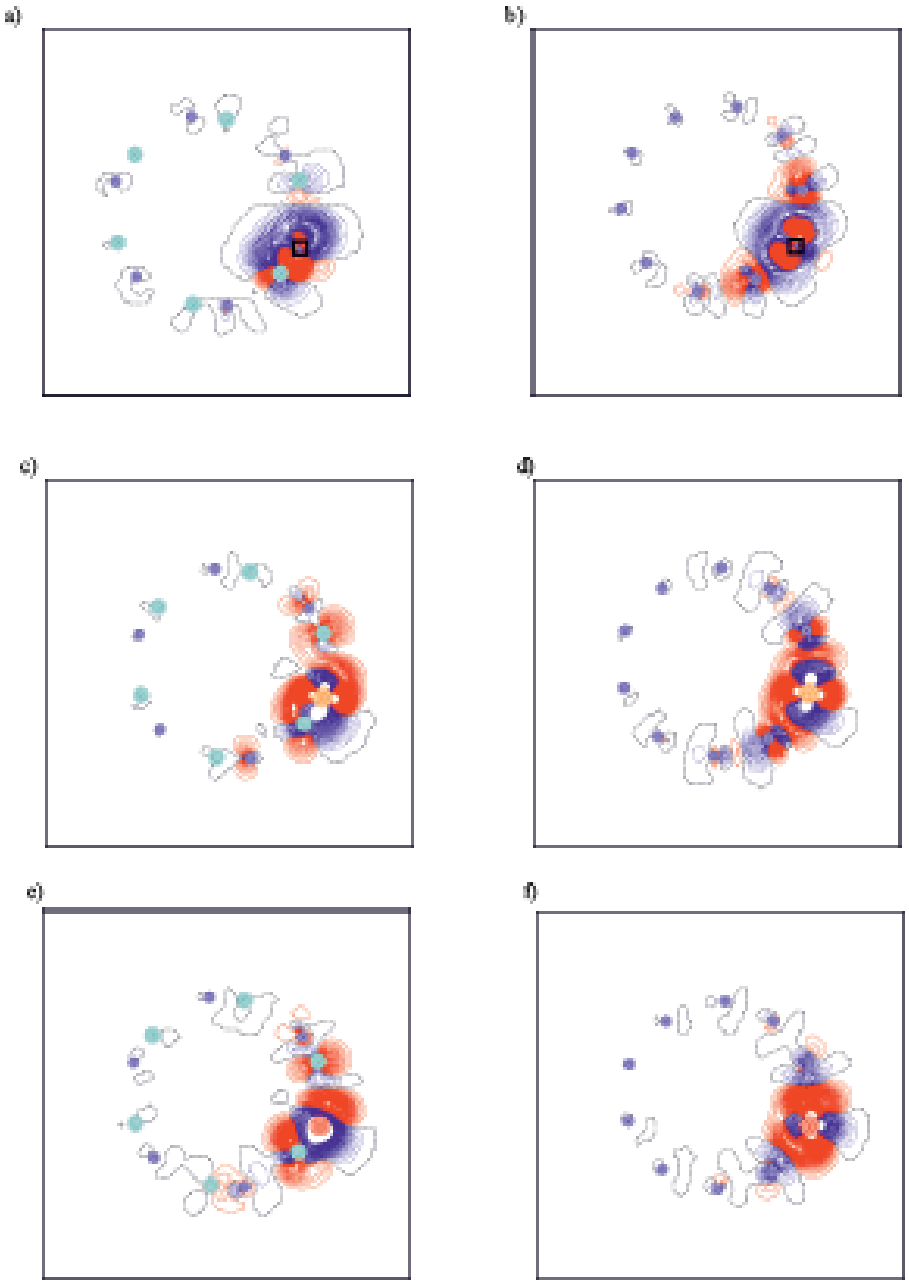

2D difference electron density plots $\Delta\rho(\mathbf{r})$ (the sum of total electron densities in the perfect BN NT and isolated defect (X) minus the sum of these densities in the isolated N atom and defective nanotube) projected onto the section planes across nanotube containing a single defect *per* supercell: *F* center upon *ac*-NT (a) and *zz*-NT (b); C_N upon *ac*-NT (c) and *zz*-NT (d); O_N upon *ac*-NT (e) and *zz* -NT (f). Dash-dot (black online) isolines correspond to the zero level. Solid (red) and dashed (blue) isolines describe positive and negative values of the difference in electron density, respectively. Isodensity curves are drawn from –0.05 to +0.05 *e* $Å^{-3}$ with increments of 0.00025 *e* $Å^{-3}$.

5a. Models and properties of BN SW NTs with single defects

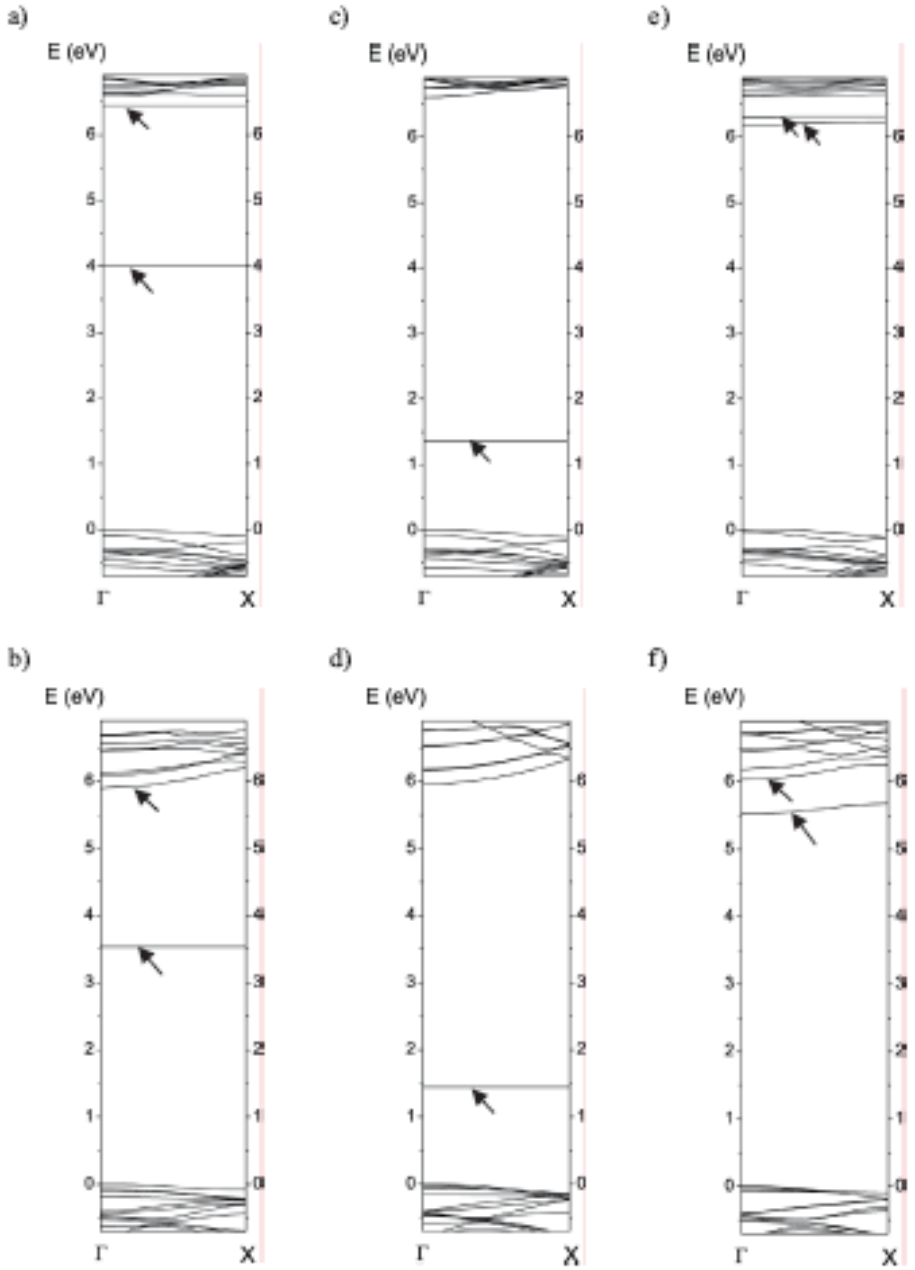

Band structures of BN nanotubes containing a single defect *per* supercell: *F* center upon *ac*-NT (a) and *zz*-NT (b); C_N upon *ac*-NT (c) and *zz*-NT (d); O_N upon *ac*-NT (e) and *zz* -NT (f). Arrows show the defect bands whereas zero level in all the energy scales is chosen at the top VB.

5a. Models and properties of BN SW NTs with single defects

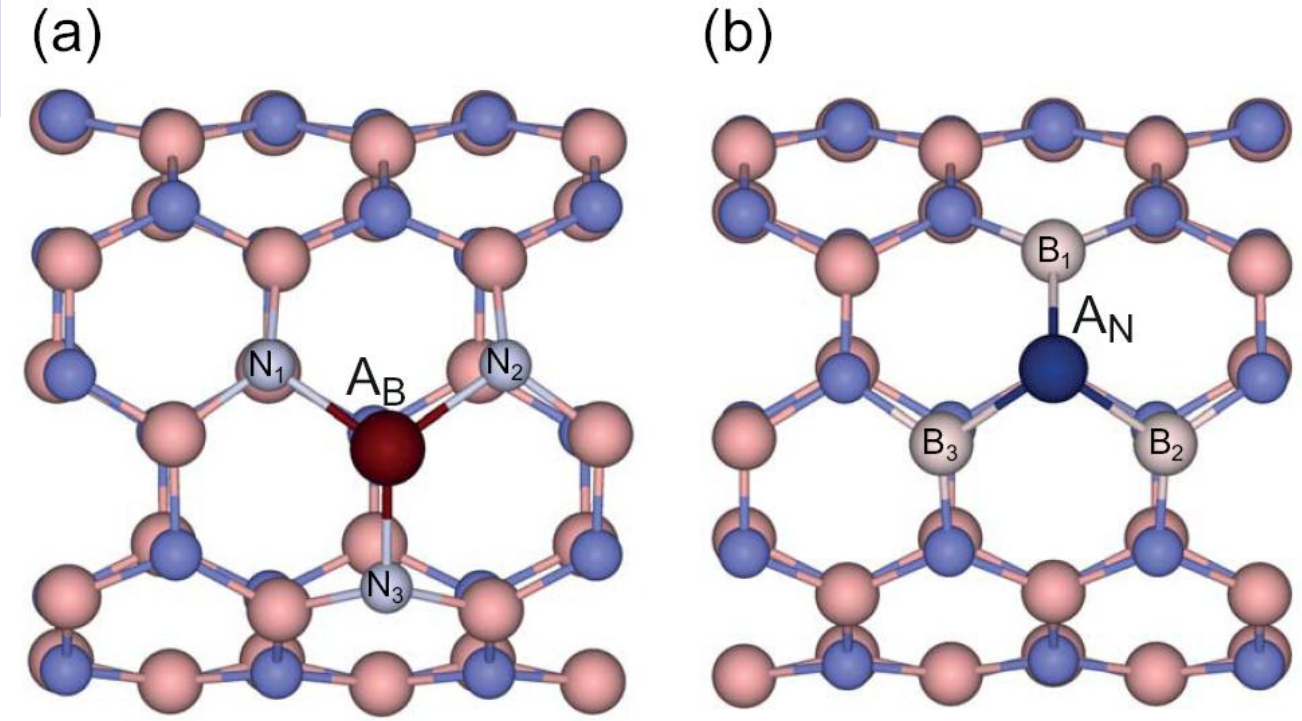

Schematic representation of the (mono)periodically repeated unit cell of the substitutional defect containing **(5,5) BN nanotube**: (a) host boron substitutes for impurity defect atom (A_B) and (b) host nitrogen substitutes for impurity defect atom (A_N). Borons are shown as blue (dark gray) balls, while nitrogens as pink (light gray) ones. Nearest to defect neighbor host atoms (h0n) are shown in dimmed colors. Substitutes were chosen to be: **A_B = Al, Ga, In and A_N = P, As, Sb**

5a. Models and properties of BN SW NTs with single defects

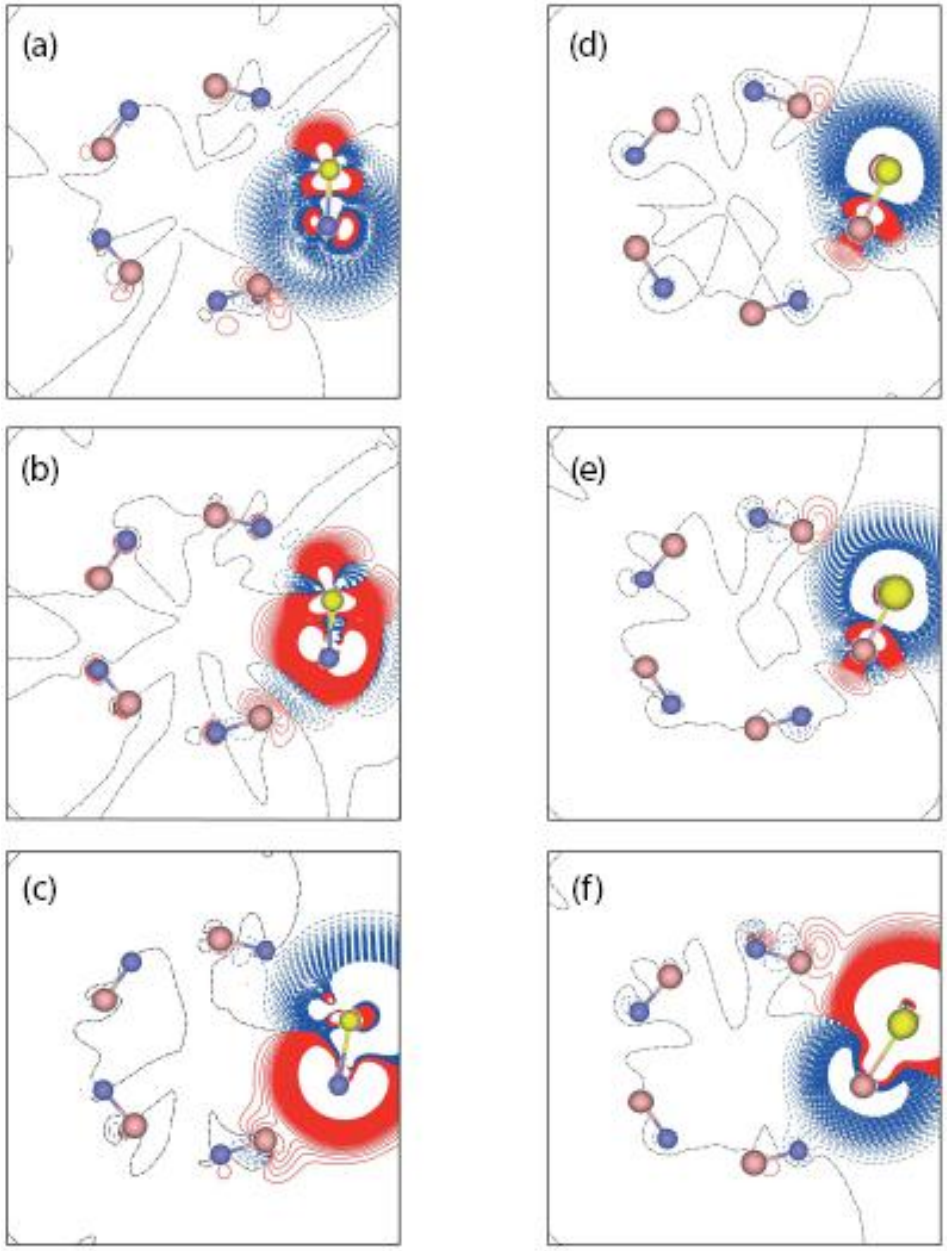

2D difference electron density plots (r) (the sum of total electron densities in the defective BN nanotube and isolated host B (or N) atom minus the sum of these densities in the isolated impurity atom (A_h, where h stands for "host" atom) and perfect nanotube) projected onto the section planes across BN nanotube containing an impurity defect per supercell: **(a) Al_B/BNNT, (b) Ga_B/BNNT, (c) In_B/BNNT, (d) P_N/BNNT, (e) As_N/BNNT, (f) Sb_N/BNNT.** Borons are shown as blue (dark gray) balls, nitrogens as pink (light gray) bals, substitutional impurity atoms (A_h) are shown in yellow (light gray). Dash-dot (black online) isolines correspond to the zero level. Solid (red) and dashed (blue) isolines describe positive and negative values of the difference in electron density, respectively. Isodensity curves are drawn from 0.01 to +0.01 e Å^{-3} with an increment of 0.0001 e Å^{-3}.

5b. Models and properties of TiO_2 SW NTs with single defects

International Conference on Functional Materials and Nanotechnologies (FM&NT2012) IOP Publishing
IOP Conf. Series: Materials Science and Engineering 38 (2012) 012057 doi:10.1088/1757-899X/38/1/012057

Ab initio modeling of sulphur doped TiO_2 nanotubular photocatalyst for water-splitting hydrogen generation

O Lisovski[1,3], S Piskunov[2,3,4], Y F Zhukovskii[4] and J Ozolins[1]
[1]Faculty of Materials Science and Applied Chemistry, Riga Technical University, Latvia
[2]Faculty of Computing, University of Latvia, Latvia
[3]Faculty of Physics and Mathematics, University of Latvia, Latvia
[4]Institute for Solid State Physics, University of Latvia, Latvia

5b. Models and properties of TiO_2 SW NTs with single defects

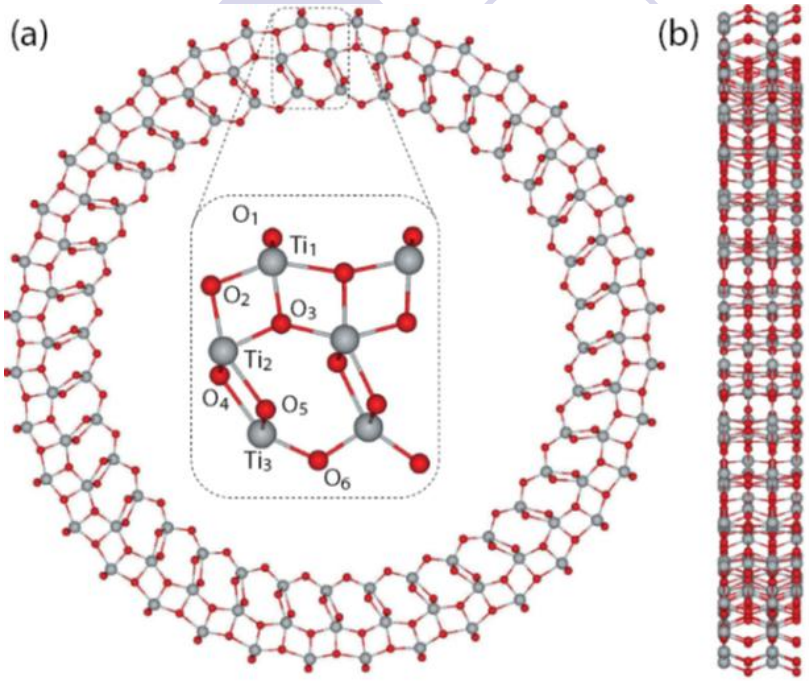

Schematic representation of the (mono)periodically repeated unit cell of the substitutional defect containing (0,36) TiO_2 nanotube: (a) front view, (b) side view.. Inset shows the 22 increased "basic" unit cell of (0,36) TiO_2 nanotube repeated by 18 rototranslational symmetry operators (rotation axis of 18- th order). Numbered are titans and oxygens that are substituted for impurity defect atoms (A_h, h stands for "host").

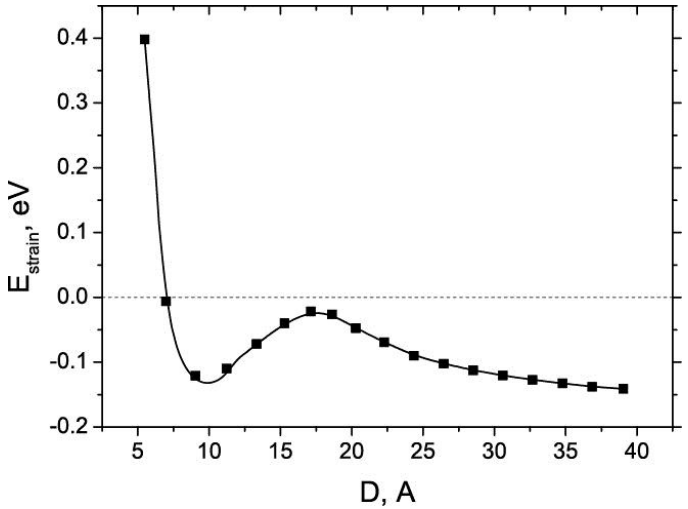

Calculated strain energies, E_{strain}, *vs.* NT diameters for (0,*n*) 9-layered (001) NT.

5b. Models and properties of TiO_2 SW NTs with single defects

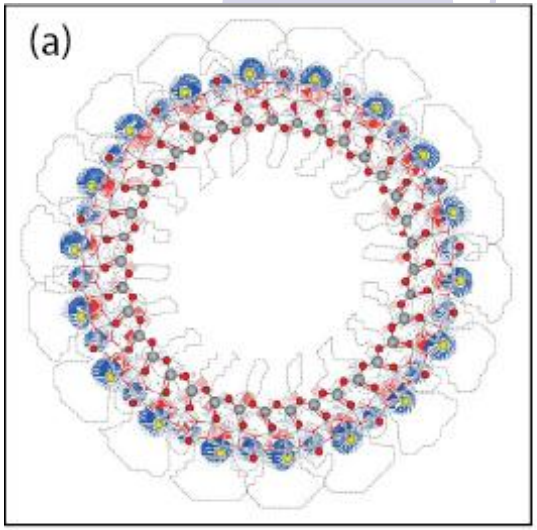

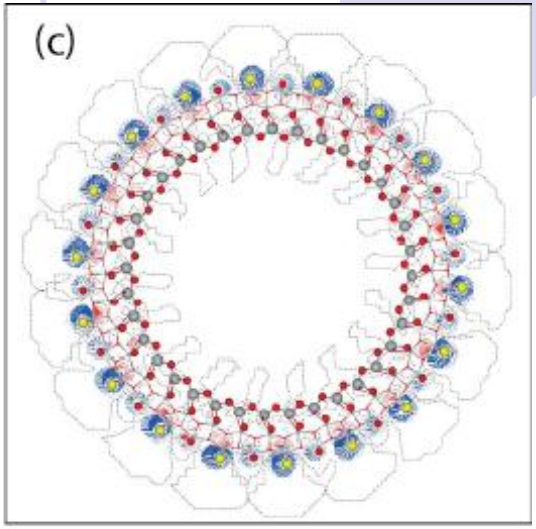

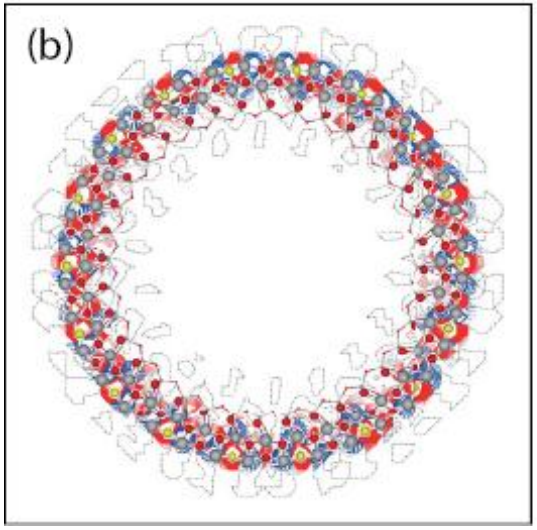

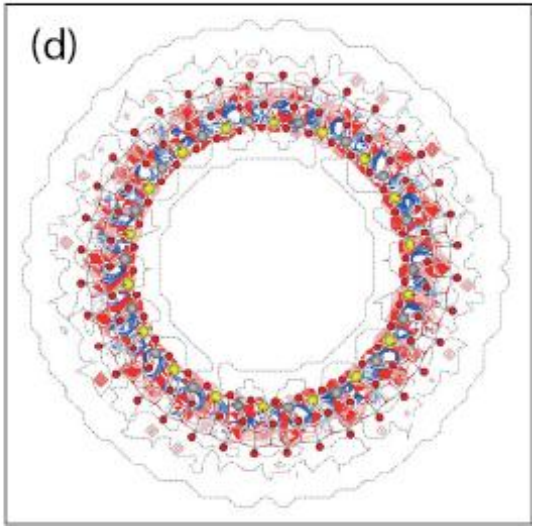

2D difference electron density plots (r) (the sum of total electron densities in the defective TiO2 nanotube and isolated host Ti (or O) atom minus the sum of these densities in the isolated impurity atom (Ah, where h stands for "host" atom) and perfect nanotube) projected onto the section planes across TiO2 nanotube containing an impurity defect per supercell: **(a) C_{O1}/TiO_2-NT, (b) N_{O2}/TiO_2-NT, (c) S_{O1}/TiO_2-NT, (d) Fe_{Ti3}/TiO_2-NT**. Ti are shown as gray balls, O as red (light gray) balls, substitutional impurity atoms (A_h) are shown in yellow (light gray). Atoms that placed outside the crossing plane are shown as balls with reduced size. Dash-dot (black online) isolines correspond to the zero level. Solid (red) and dashed (blue) isolines describe positive and negative values of the difference in electron density, respectively. Isodensity curves are drawn from 0.05 to +0.05 *e* $Å^{-3}$ with an increment of 0.0005 *e* $Å^{-3}$.

5c. Models and properties of $SrTIO_3$ SW NTs with single defects

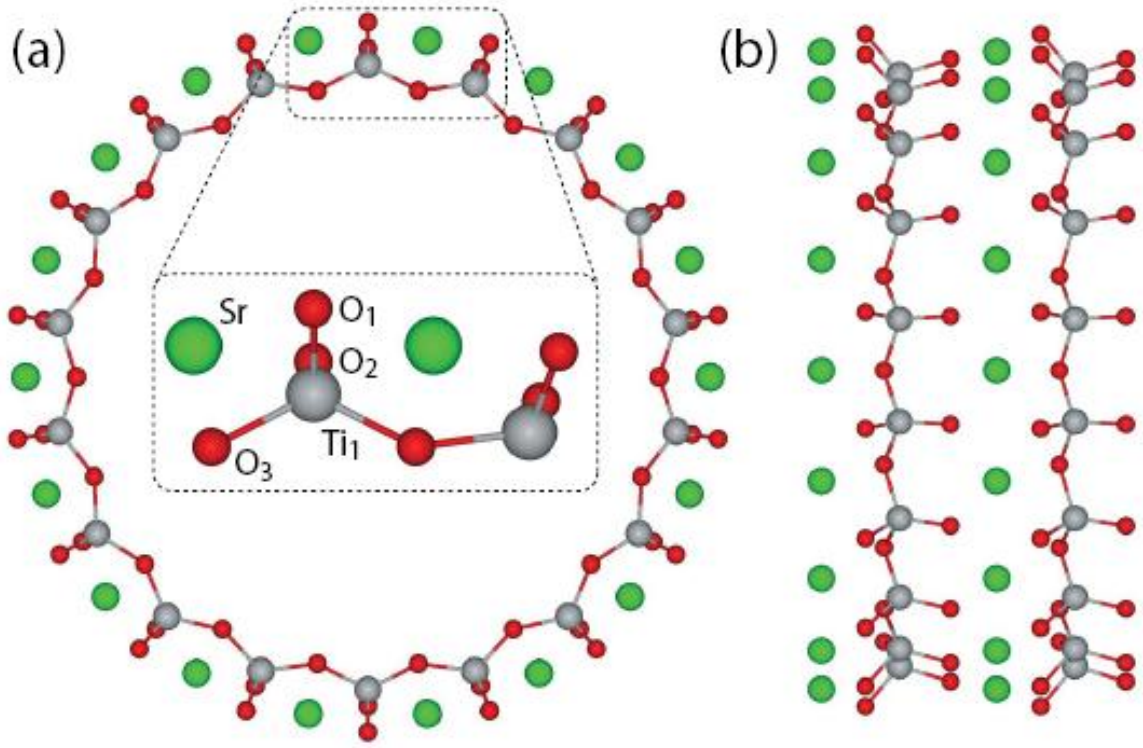

Schematic representation of the (mono)periodically repeated unit cell of the substitutional defect containing (18,0) $SrTiO_3$ nanotube: (a) front view, (b) side view. Ti are shown as gray balls, oxygens as red (light gray) balls, and strontiums as green (gray) ones. Inset shows the 22 increased ”basic” unit cell of (18,0) $SrTiO_3$ nanotube repeated by 9 rototranslational symmetry operators (rotation axis of 9-th order). Numbered atoms are titans and oxygens that are substituted for impurity defect atoms (A_h, h stands for ”host”).

5c. Models and properties of $SrTiO_3$ SW NTs with single defects

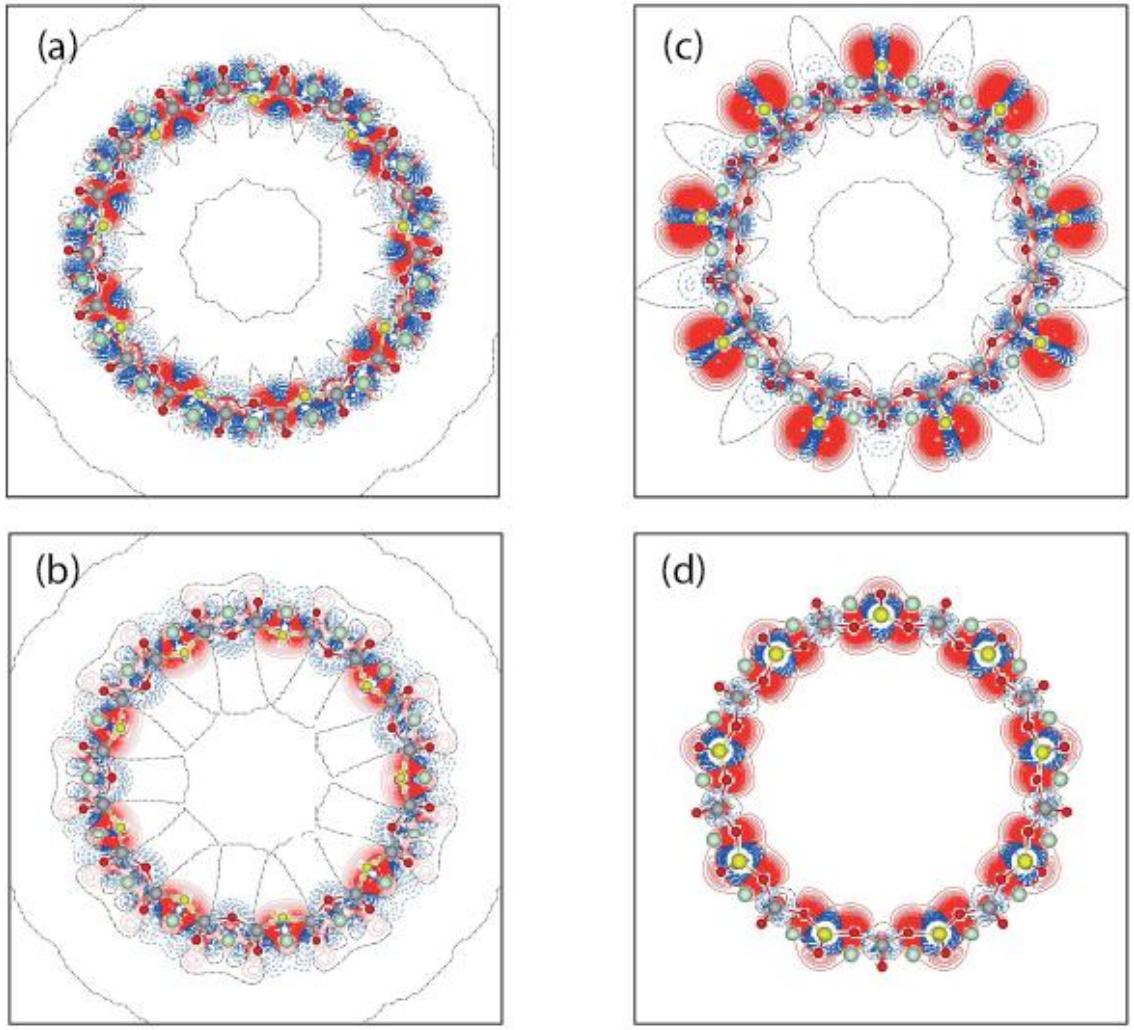

2D difference electron density plots (r) (the sum of total electron densities in the defective SrTiO3 nanotube and isolated host Ti (or O) atom minus the sum of these densities in the isolated impurity atom (Ah, where h stands for "host" atom) and perfect nanotube) projected onto the section planes across $SrTiO_3$ nanotube containing an impurity defect per supercell: **(a) C_{O3} /$SrTiO_3$ NT, (b) N_{O3} /$SrTiO_3$ NT, (c) S_{O1} /$SrTiO_3$ NT, (d) Fe_{Ti1}/$SrTiO_3$ NT.** Ti atoms are shown as gray balls, O as red (light gray) balls, Sr as green (gray), substitutional impurity atoms (A_h) are shown in yellow (light gray). Atoms that placed outside the crossing plane are shown in dimmed colors. Dash-dot (black online) isolines correspond to the zero level. Solid (red) and dashed (blue) isolines describe positive and negative values of the difference in electron density, respectively. Isodensity curves are drawn from 0.05 to +0.05 e Å^{-3} with an increment of 0.0005 e Å^{-3}.

5. Summary and predictions

1. The results of defect modeling in boron nitride, titanium dioxide and strontium titanate nanotubes obtained using first-principles calculations based on hybrid density functional theory are analyzed.
2. The variations in formation energies obtained for equilibrium defective nanostructures allow us to predict the most stable compositions, irrespective of the changes in growth conditions.
3. Calculated charge density maps of the different tubular nanostructures containing extrinsic substitutional impurity atoms highlighted changes in the charge distribution caused by doping. Inspecting the isodensity plots one may conclude that increased covalency in defect-host atom bonds may lead to an enhancement of adsorption properties. This would imply that defective NTs can be used in gas-sensing devices.
4. The presence of isoelectronic impurities significantly affects the band structure of NTs under study, which must be taken into account when constructing nanoelectronic devices based on these nanotubes.
5. Defect levels positioned inside the optical band gap of defective NTs makes them attractive for band gap engineering in, for example, photocatalytic applications. All the mentioned effects can be observed by optical and photoelectron spectroscopy methods, as well as by measuring electrical properties of the nanotubes.

6. Models and properties of perfect TiO_2 NWs

6. Models and properties of TiO_2 NWs

THE JOURNAL OF PHYSICAL CHEMISTRY C

Article

pubs.acs.org/JPCC

J. Phys. Chem. C 2012, 116, 13395−13402

Symmetry and Stability of the Rutile-Based TiO_2 Nanowires: Models and Comparative LCAO-Plane Wave DFT Calculations

R. A. Evarestov,*[,†] D. B. Migas,[‡] and Yu. F. Zhukovskii[§]

[†]Department of Quantum Chemistry, St. Petersburg State University, 26 Universitetsky Avenue, Petrodvorets 198504, Russia

[‡]Belarusian State University of Informatics and Radioelectronics, 6 P. Browka Str., Minsk, 220013, Belarus

[§]Institute of Solid State Physics, University of Latvia, 8 Kengaraga Str., Riga LV-1063 Latvia

International Conference on Functional Materials and Nanotechnologies (FM&NT2012) IOP Publishing

IOP Conf. Series: Materials Science and Engineering 38 (2012) 012005 doi:10.1088/1757-899X/38/1/012005

Ab initio simulations on rutile-based titania nanowires

Yu F Zhukovskii[1,3], R A Evarestov[2]

[1]Institute of Solid State Physics, University of Latvia, 8 Kengaraga Str., LV-1063, Riga, Latvia.

[2]Department of Quantum Chemistry, St. Petersburg State University, 26 Universitetsky Ave., 198504, Petrodvorets, Russia.

E-mail: quantzh@latnet.lv

6. Models and properties of TiO_2 NWs

rod group *Pmmm* (D_{2h} point symmetry)

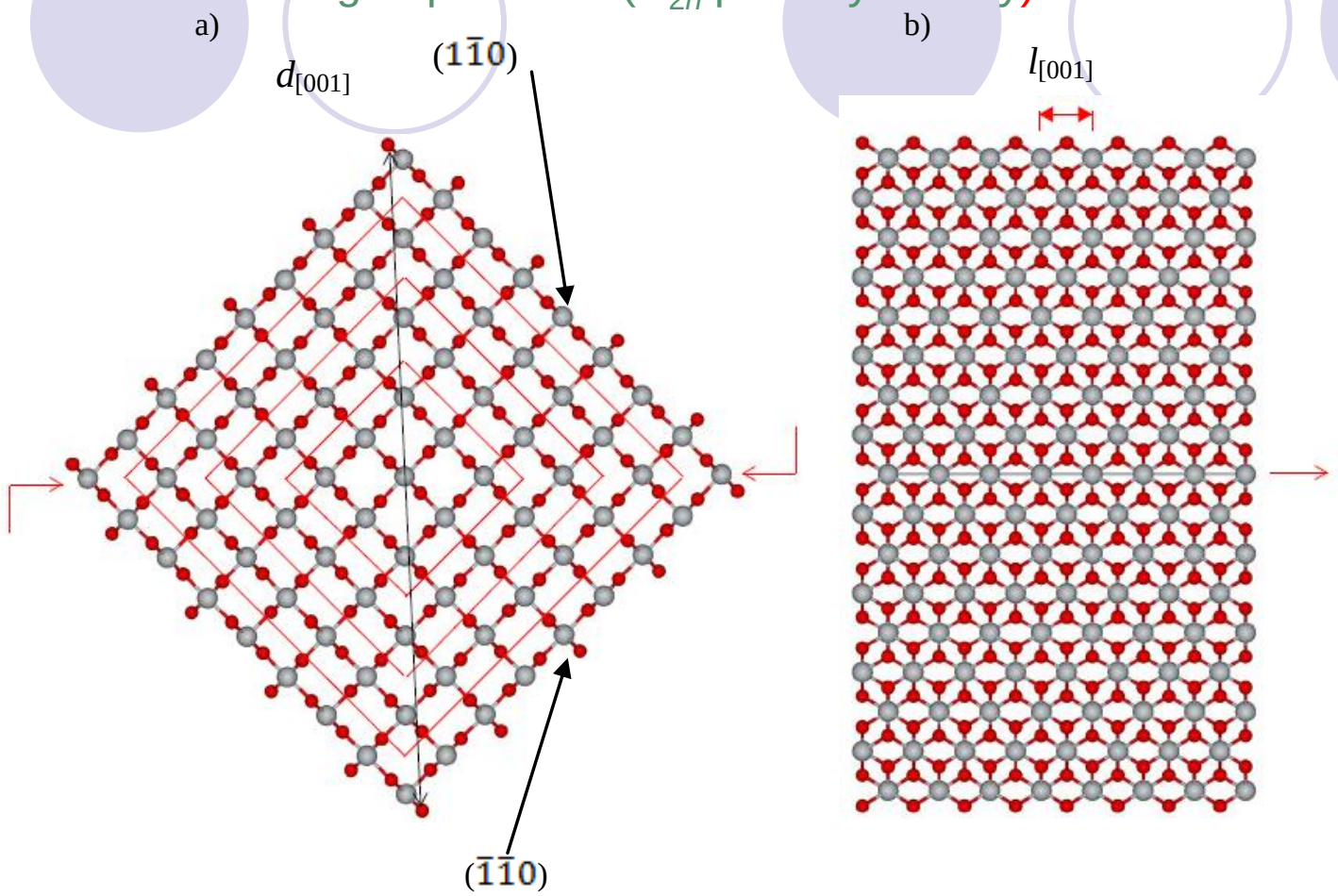

Figure 2. Cross sectional (a) and lateral (b) images of non-optimized large rutile-based titania [001]-oriented NW-1 possessing the Ti atom-centered D_{2h} symmetry axis and containing 81 formula units *per* NW unit cell (UC), with aside $(1\bar{1}0)$ and $(\bar{1}\bar{1}0)$ facets shown in Fig. 2b. Red rhombs in Fig. 2a show borders for prism models of middle, small and smallest TiO_2 NWs (49, 25 and 9 formula units *per* UC, respectively). Diameter of a nanowire is shown by the twice-terminated arrow ($d_{[001]}$) while its period (length of UC) is shown in Fig. 2b as $l_{[001]}$.

6. Models and properties of TiO_2 NWs

rod group *Pmmm* (D_{2h} point symmetry)

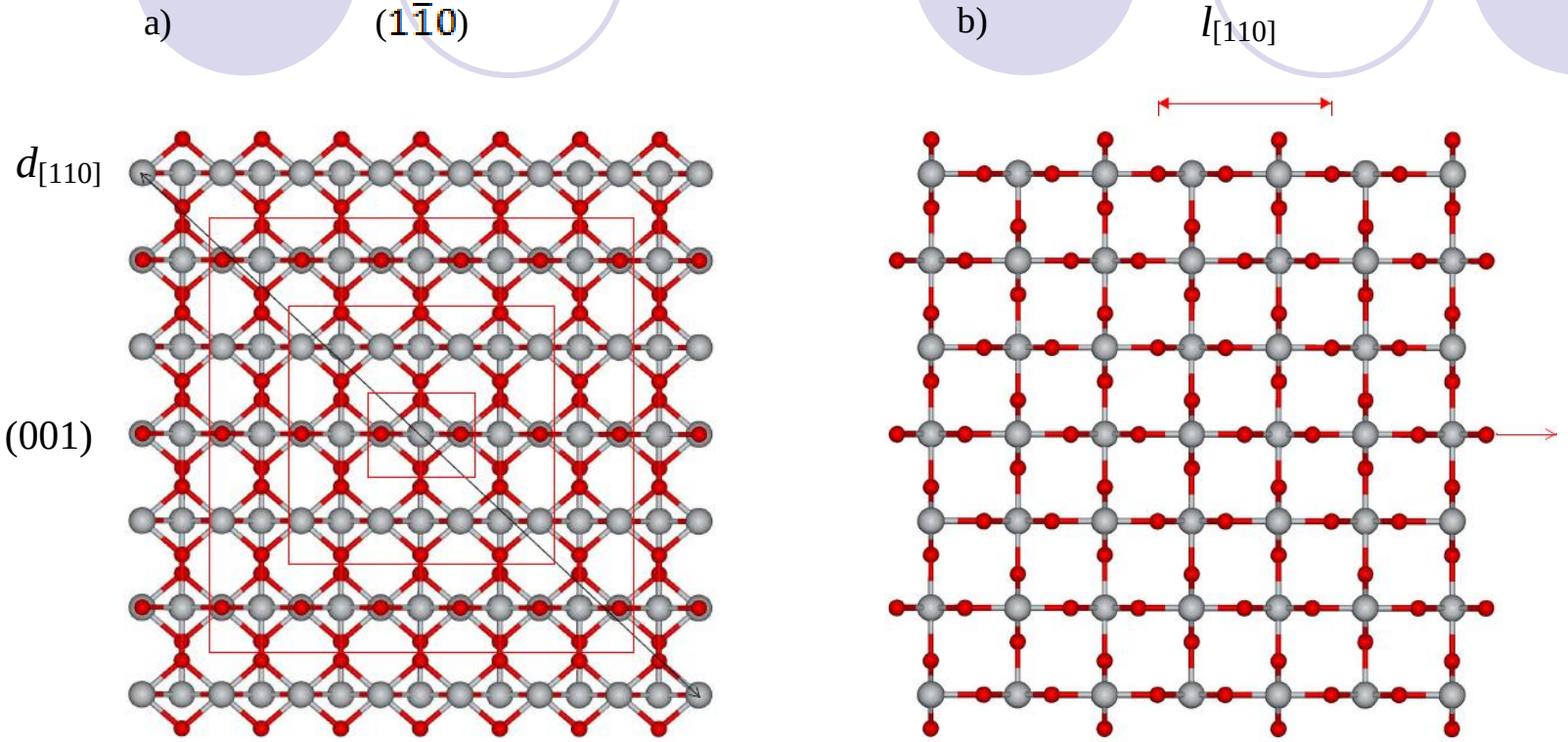

Figure 3. Cross sectional (a) and lateral (b) images of the non-optimized large rutile-based titania [110]-oriented NW-2 possessing the Ti atom-centered D_{2h} symmetry axis and containing 105 formula units *per* NW UC, with aside (001) and (1$\bar{1}$0) facets (the former is shown in Fig. 3b). Red quasi-square rectangles in Fig. 3a show borders for prism models of middle, small and smallest TiO_2 NWs (55, 21 and 3 formula units *per* UC, respectively). Diameter of a nanowire is shown by the twice-terminated arrow ($d_{[110]}$) while its period (length of UC) is shown in Fig. 3b as $l_{[110]}$.

6. Models and properties of TiO_2 NWs

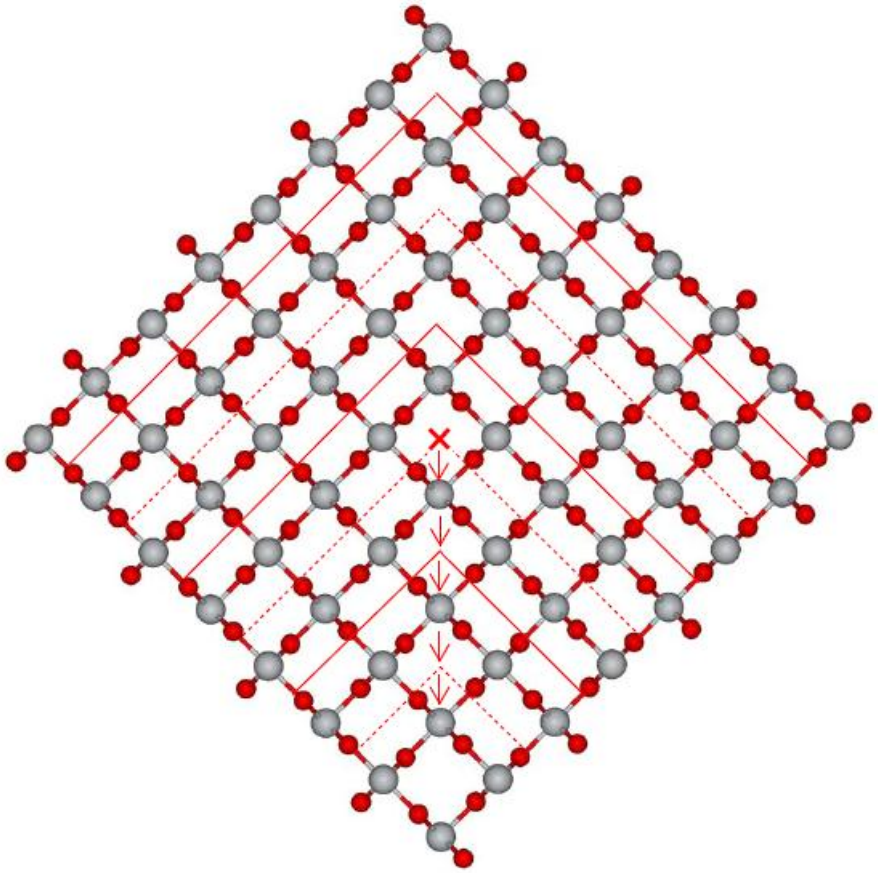

Figure 4. Across image of non-optimized large rutile-based titania <001> nanowire possessing hollow-centered C_{4h} screw axis (its track is shown by cross) and containing 64 formula units *per* NW UC. Small arrows show shift directions and lengths for NW axis during nanowire transformation to alternating Ti atom-centered and hollow-centered configurations. Two adjacent sides of rhombs imaged by solid lines show borders for prism models of Ti atom-centered middle, small and smallest TiO_2 NWs (with 49, 25 and 9 formula units *per* UC) while those limited by dashed lines correspond to hollow-centered middle, small and smallest TiO_2 NWs (36, 16 and 4 formula units *per* UC). Directions of two other rhombic sides for all <001> NW configurations described here coincide with the two lower sides shown in across image.

6. Models and properties of TiO_2 NWs

$4_2/m$ rod group (C_{4h} point symmetry)

$Pm11$ rod group (C_s point symmetry)

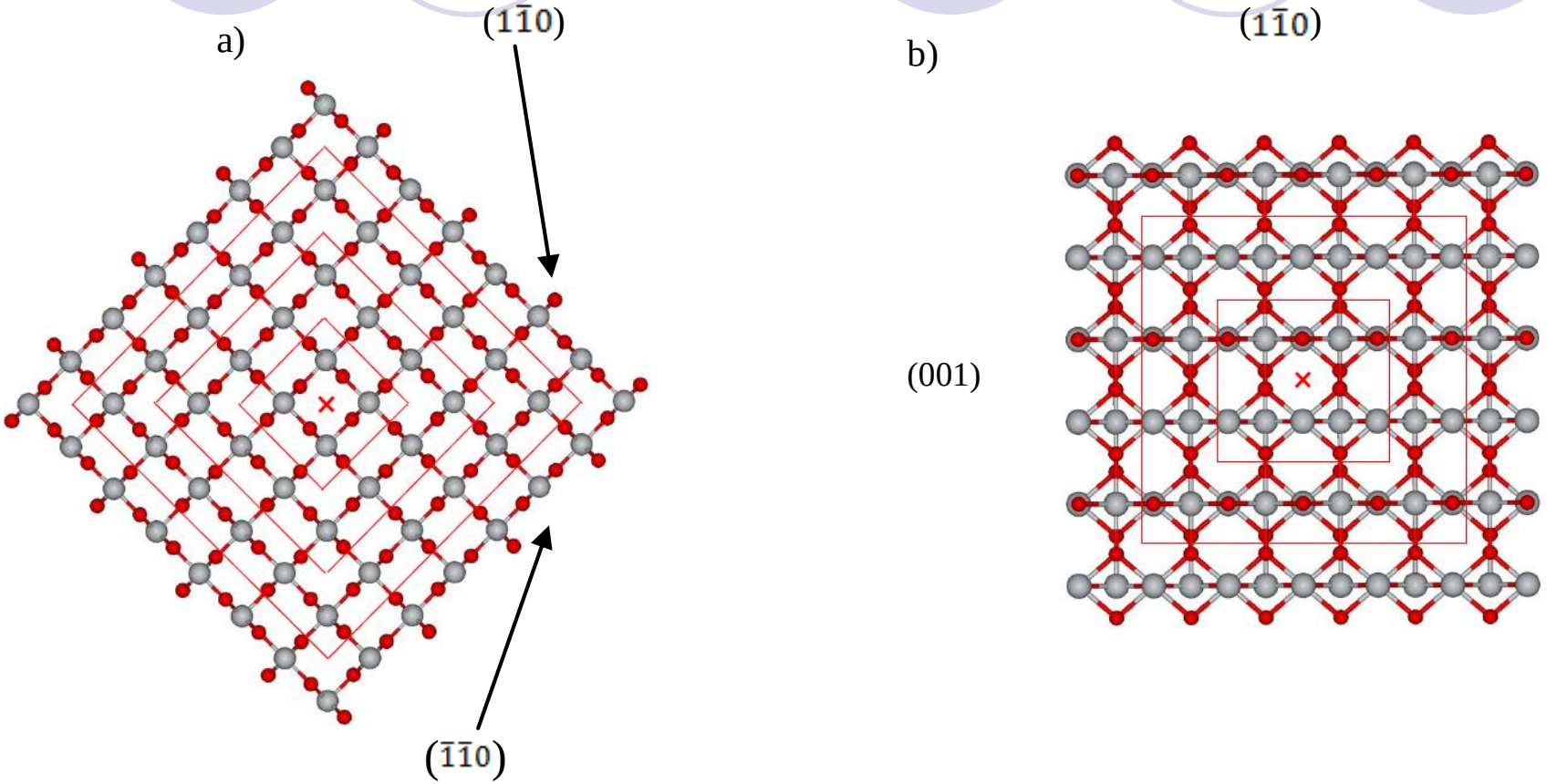

Figure 5. Cross sections of [001]-oriented (a) and [110]-oriented TiO_2 NWs (b) containing 64 *vs.* 78 formula units *per* large NW unit cells, respectively. Rhombs and rectangles show borders for prism models of middle and small TiO_2 NWs (with 36 *vs.* 36, 16 *vs.* 10 plus 4 formula units *per* unit cells, respectively). Figure indicates indices of facets for both nanowires. NW centers are shown as crosses.

6. Models and properties of TiO_2 NWs

1. Due to a variety of promising applications, single-crystalline titania nanowires (TiO_2 NWs) attract enhanced attention in modern nanotechnology. Rutile-based TiO_2 NWs are modeled as 1D structures cut from 3D crystal along [001] and [110] crystallographic axes. These nanowires in the case of Ti-atom centered symmetry axes are described using the same rod group *Pmmm* (D_{2h} point symmetry) for both [001] and [110] oriented NWs (Figs. 2, 3). In the case of hollow site-centered symmetry axes, NW symmetry depends on the orientation of crystallographic axes (Fig. 5): (*i*) [001] nanowires are described by non-symmorphic $4_2/m$ rod group (C_{4h} point symmetry); (*ii*) [110] nanowires can be described by a symmetrically poor *Pm11* rod group characterized by presence of mirror plane only (C_s point symmetry).

2. The rutile-based TiO_2 NWs clearly display only the energetically preferable {110} facets in the case of their [001] orientation as well as the alternating {110} and {001} facets in the case of [110] NW orientation, in accordance with the Wulff construction formalism*. *Ab initio* calculations have been performed on both nanowire types. Two main reasons cause a necessity to simulate [001] and [110] NW orientations: (*i*) the thermodynamic contribution to nanowire stability is independent of NW morphology for diameters more than 10 nm as mainly synthesized experimentally (while *ab initio* calculations can be performed only for nanowires with diameters < 5 nm); (*ii*) the interface between a catalytic substrate and a nucleation titania seed should display rather low energy to surpass the nucleation barrier. This is why the [110]-oriented rutile-based TiO_2 NWs were synthesized more frequently so far.

*Herring, C. Phys. Rev. 1951, 82, 87-93.

6. Models and properties of TiO_2 NWs

Table 2. Properties of optimized [001] Ti-atom centered titania nanowire (Fig. 2).

Nanowire size (number N_{UC} of TiO_2 formula units *per* UC)	Initial diameter of NW d_{NW}, Å	Optimized NW diameter (its change) d_{NT}, Å (δd_{NT}, %)	Initial length of NW UC l_{NW}, Å	Optimized NW period (its change) l_{NW}, Å (δl_{NT}, %)	Surface energy of nanowire E_{surf}, J/m^2	Band gap (its change from that of bulk, Table 1) $\Delta\varepsilon_g$, eV ($\delta\varepsilon_g$, %)
PBE						
9 (smallest)	11.122	11.493 (+3.33)	2.980	2.911 (-2.37)	1.023	1.04 (-40.38)
25 (small)	20.240	20.711 (+2.32)		2.944 (-1.22)	0.906	1.51 (-13.25)
49 (middle)	29.400	29.941 (+1.84)		2.957 (-0.78)	0.842	1.57 (-9.67)
81 (large)	38.670	39.270 (+1.55)		2.963 (-0.57)	0.789	1.60 (-8.18)
PBE0						
9 (smallest)	10.979	11.268 (+2.63)	2.964	2.881 (-2.88)	1.072	3.15 (-21.59)
25 (small)	19.980	20.476 (+2.48)		2.927 (-1.26)	0.971	3.61 (-6.09)
49 (middle)	29.023	29.594 (+1.97)		2.940 (-0.82)	0.914	3.70 (-3.51)
81 (large)	38.174	38.712 (+1.41)		2.946 (-0.61)	0.861	3.74 (-2.41)

$$E_{surf} = (E_{NW\_UC} - n_{FU}E_{bulk})/S$$

6. Models and properties of TiO_2 NWs

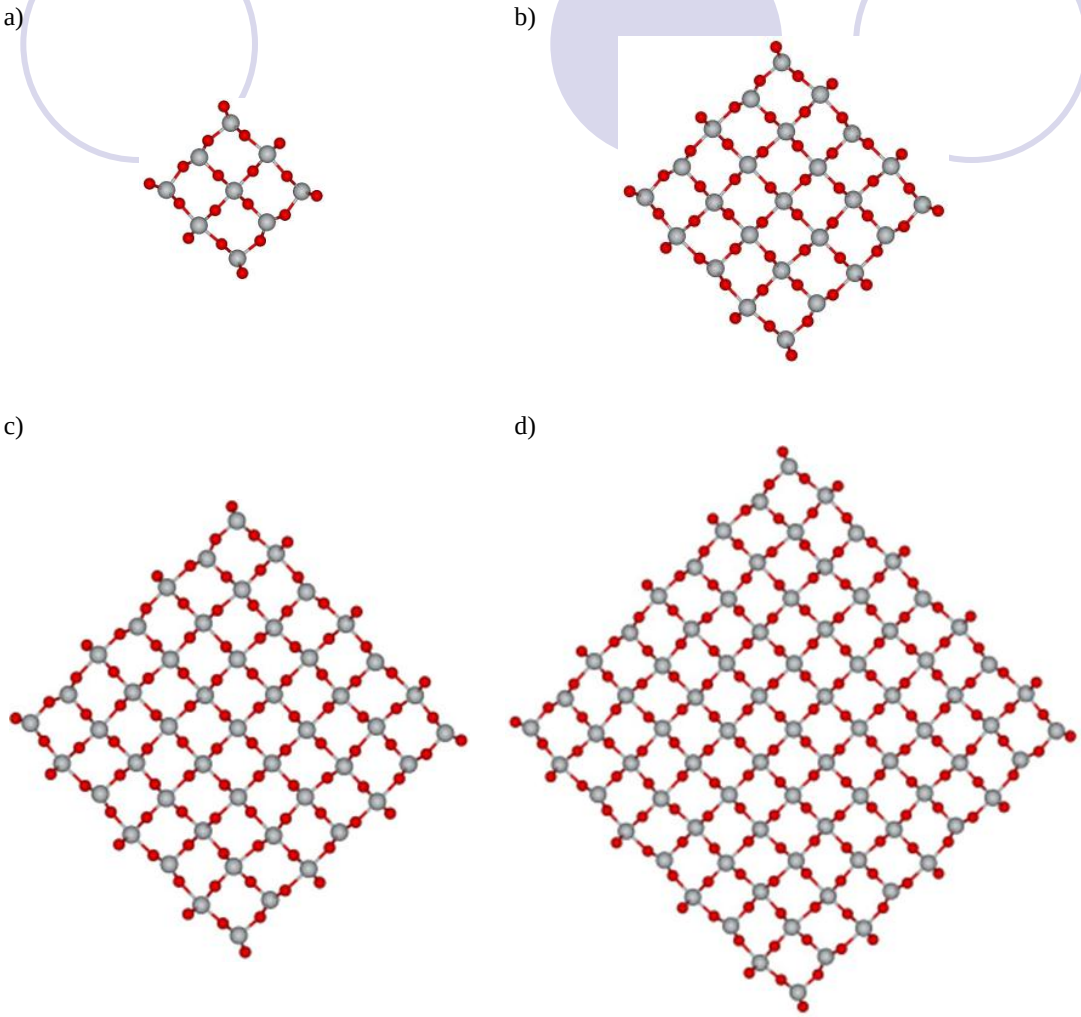

Figure 6. Cross sectional views of optimized Ti-atom centered titania [001] NWs of smallest (a), small (b), middle (c) and large (d) diameters calculated using DFT-LCAO method (parameters of relaxation are present in Table 2). Section planes for present images are chosen the same as in Figures 2.

6. Models and properties of TiO_2 NWs

Table 3. Properties of optimized [001] hollow-centered titania nanowire (Fig. 5a).

Nanowire size (number N_{UC} of TiO_2 formula units *per* UC)	Initial diameter of NW d_{NW}, Å	Optimized NW diameter (its change) d_{NT}, Å (δd_{NT}, %)	Initial length of NW UC l_{NW}, Å	Optimized NW period (its change) l_{NW}, Å (δl_{NT}, %)	Surface energy of nanowire E_{surf}, J/m^2	Band gap (its change from that of bulk, Table 1) $\Delta\varepsilon_g$, eV ($\delta\varepsilon_g$, %)
PBE						
4 (smallest)	6.632	6.872 (+3.61)	2.980	2.893 (-3.01)	1.057	3.40 (95.40)
16 (small)	15.672	16.094 (+2.69)		2.937 (-1.46)	0.854	2.34 (34.48)
36 (middle)	24.818	25.327 (+2.05)		2.954 (-0.88)	0.773	2.24 (28.74)
64 (large)	33.984	34.567 (+1.72)		2.962 (-0.61)	0.746	2.03 (16.67)
PBE0						
4 (smallest)	6.545	6.789 (+3.73)	2.964	2.876 (-3.06)	1.106	4.53 (18.28)
16 (small)	15.466	15.892 (+2.75)		2.919 (-1.54)	0.873	4.09 (6.79)
36 (middle)	24.492	25.007 (+2.10)		2.934 (-1.02)	0.842	3.98 (3.92)
64 (large)	33.538	34.140 (+1.80)		2.945 (-0.65)	0.829	3.93 (2.61)

$$E_{surf} = (E_{NW\_UC} - n_{FU}E_{bulk}) / S$$

6. Models and properties of TiO_2 NWs

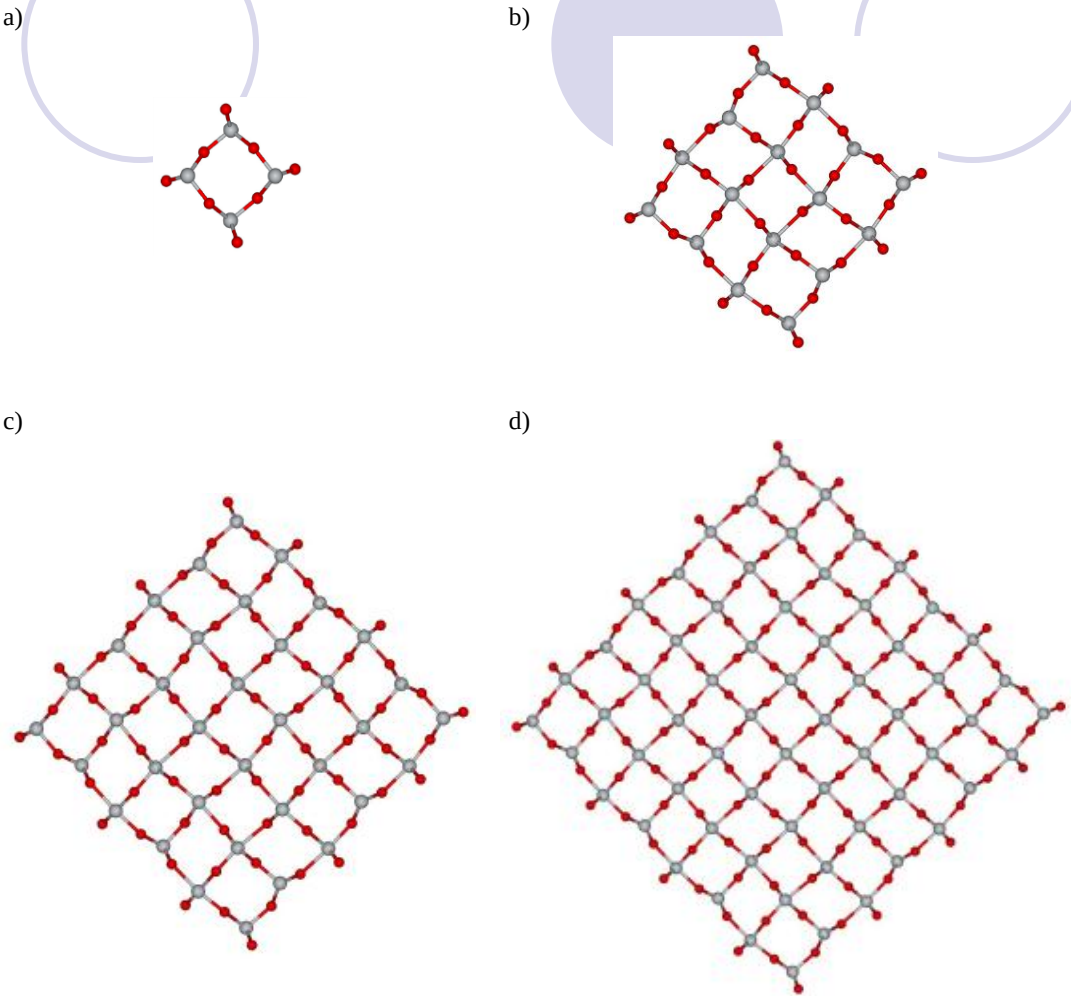

Figure 7. Cross sectional views of optimized hollow site centered titania [001] NWs of smallest (a), small (b), middle (c) and large (d) diameters calculated using DFT-LCAO method (parameters of relaxation are present in Table 3). Section planes for present images are chosen the same as in Figures 2.

6. Models and properties of TiO_2 NWs

Table 4. Properties of optimized [110] Ti-atom centered titania nanowire (Fig. 3).

Nanowire size (number N_{UC} of TiO_2 formula units *per* UC)	Initial diameter of NW d_{NW}, Å	Optimized NW diameter (its change) d_{NT}, Å (δd_{NT}, %)	Initial length of NW UC l_{NW}, Å	Optimized NW period (its change) l_{NW}, Å (δl_{NT}, %)	Surface energy of nanowire E_{surf}, J/m^2	Band gap (its change from that of bulk, Table 1) $\Delta\varepsilon_g$, eV ($\delta\varepsilon_g$, %)
PBE						
3 (smallest)	2.958	2.882 (-2.64)	6.572	6.251 (-5.14)	2.771	1.60 (-8.12)
21 (small)	10.996	11.237 (+2.19)		6.377 (-3.06)	1.453	1.46 (-16.47)
55 (middle)	19.683	20.094 (+2.09)		6.424 (-2.30)	1.341	1.61 (-7.52)
105 (large)	28.431	28.966 (+1.88)		6.452 (-1.86)	1.287	1.64 (-5.88)
PBE0						
3 (smallest)	2.920	2.846 (-2.60)	6,487	6.210 (-4.46)	3.117	3.67 (-4.36)
21 (small)	10.852	11.125 (+2.52)		6.315 (-2.72)	1.520	3.65 (-4.93)
55 (middle)	19.430	19.907 (+2.45)		6.356 (-2.06)	1.462	3.76 (-1.86)
105 (large)	28.066	28.689 (+2.22)		6.382 (-1.65)	1.418	3.79 (-1.06)

$$E_{surf} = (E_{NW\_UC} - n_{FU}E_{bulk}) / S$$

6. Models and properties of TiO_2 NWs

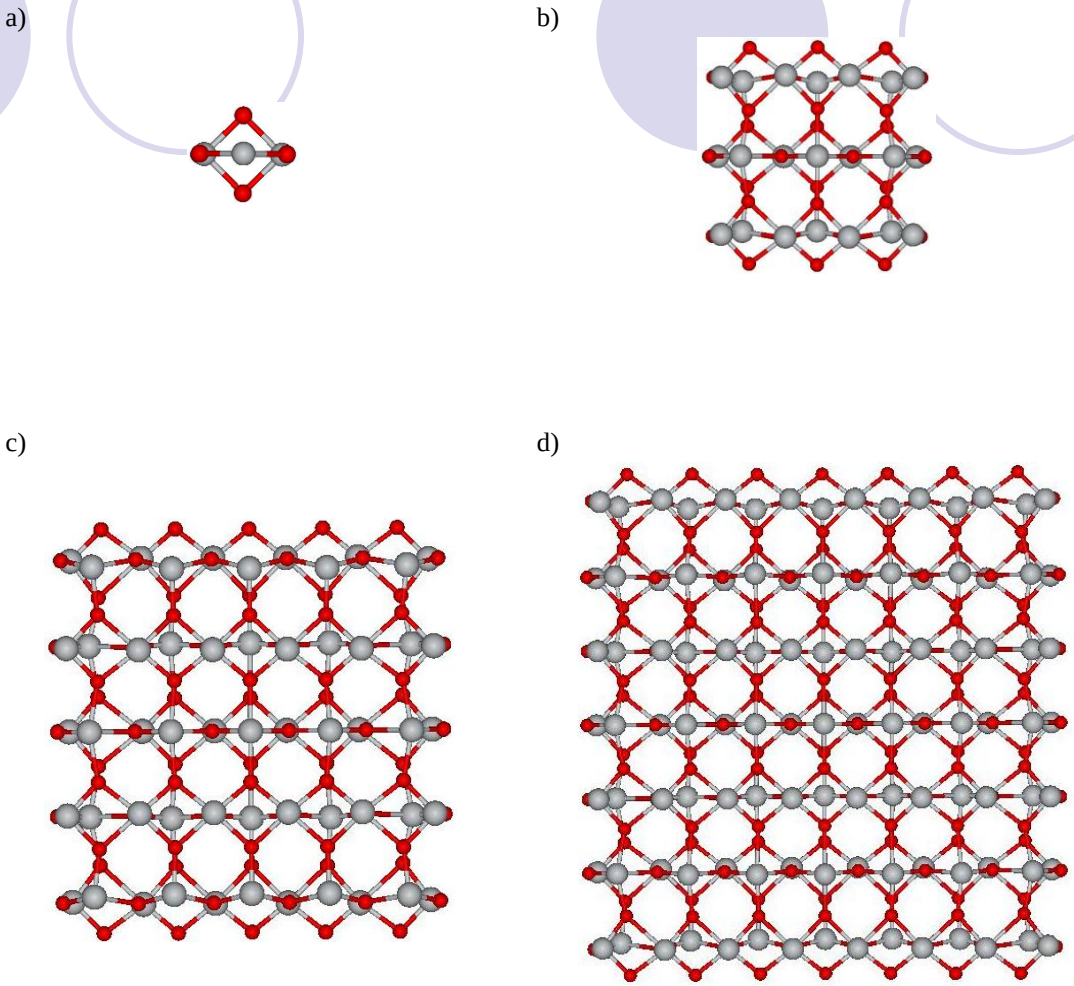

Figure 8. Cross sectional views of the optimized Ti-atom centered titania [110] NW of smallest (a), small (b), middle (c) and large (d) diameters calculated using DFT-LCAO method (parameters of relaxation are present in Table 4). Section planes for present images are chosen the same as in Figure 3.

6. Models and properties of TiO_2 NWs

Table 5. Properties of optimized [110] hollow-centered titania nanowire (Fig. 5b).

Nanowire size (number N_{UC} of TiO_2 formula units *per* UC)	Initial diameter of NW d_{NW}, Å	Optimized NW diameter (its change) d_{NT}, Å (δd_{NT}, %)	Initial length of NW UC l_{NW}, Å	Optimized NW period (its change) l_{NW}, Å (δl_{NT}, %)	Surface energy of nanowire E_{surf}, J/m^2	Band gap (its change from that of bulk, Table 1) $\Delta\varepsilon_g$, eV ($\delta\varepsilon_g$, %)
PBE						
10 (small)	6.748	6.954 (+3.06)	6.572	6.264 (-4.92)	1.651	2.11 (21.26)
36 (middle)	15.326	15.483 (+1.02)		6.371 (-3.15)	1.362	1.91 (9.77)
78 (large)	24.054	24.261 (+0.86)		6.424 (-2.30)	1.283	1.85 (6.32)
PBE0						
10 (small)	6.659	6.861 (+3.03)	6.487	6.208 (-4.49)	1.886	4.25 (10.97)
36 (middle)	15.125	15,472 (+2.30)		6.311 (-2.79)	1.479	4.12 (7.57)
78 (large)	23.738	24.224 (+2.05)		6.358 (-2.03)	1.391	4.03 (5.22)

$$E_{surf} = (E_{NW\_UC} - n_{FU}E_{bulk}) / S$$

6. Models and properties of TiO_2 NWs

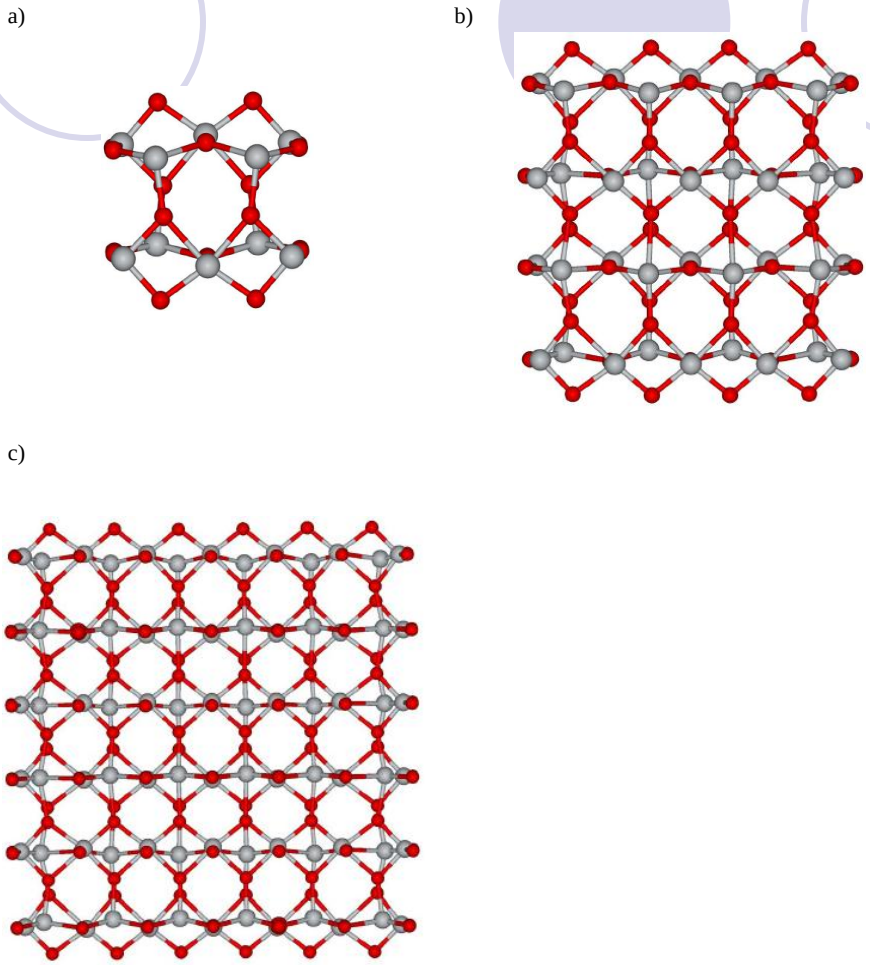

Figure 9. Cross sectional views of the optimized hollow site centered titania [110] NW of small (a), middle (b) and large (c) diameters calculated using DFT-LCAO method (parameters of relaxation are present in Table 5). Section planes for present images are chosen the same as in Figure 3.

6. SUMMARY AND PREDICTIONS

1. In this study, the rod group formalism has been applied, to construct models for bulk-like titania nanowires (NWs) cut from the rutile-based 3D crystal along the direction of a chosen crystallographic symmetry axis. We have considered both Ti atom- and hollow site centered axes. Such a conclusion requires an additional study as the calculations of the surface energy for both types of NWs were performed for the diameter dependence of the total energy. However, the properties of rutile-based nanowires are both the size and shape dependent.

2. Our comparative *ab initio* calculations clearly demonstrate that energetically preferable titania nanowires in the rutile phase (without hydrogen passivation and presence of vacancies) display only the {110} facets in the case of their [001] orientation and both the {110} and {001} facets in the case of their [110] orientation. We have also shown morphology to affect stability of TiO_2 NWs at very small diameters (< 3 Å) while at larger diameters its role is attenuated. This is well illustrated by values of surface energies.

3. Both *PBE* and *PBE0* methods have been used for calculations on large scale key properties of defectless rutile titania bulk as well as on structural and electronic properties depending on orientation, shape and diameter of TiO_2 [001] and [110] NWs. Since a few hybrid functionals are available for the *CRYSTAL-09* calculations, we have performed the large-scale *PBE0* calculations on titania nanowires, to obtain more realistic values of band gaps for both titania bulk and nanowires.

4. Values of d_{NW} slightly increase whereas E_{surf} and l_{NW} are found to be reduced after NW geometry optimization, except for the thinnest and rater unstable [110] NW (d_{NW} ~ 3 Å). The larger is NW diameter, the closer its geometry parameters as well as the band gap to those of rutile-based TiO_2 bulk. We have established a qualitative correlation between geometry parameters of DFT-LCAO *PBE* and *PBE0* calculations on both titania bulk and nanowires while band gaps drastically differ.

ACKNOWLEDGEMENTS

S. Piskunov has been supported by:

IEGULDĪJUMS TAVĀ NĀKOTNĒ

ESF
EIROPAS SOCIĀLAIS FONDS

EIROPAS SAVIENĪBA

Eiropas Sociālā fonda projekts
“Datorzinātnes pielietojumi un tās saiknes ar kvantu fiziku”
Nr.2009/0216/1DP/1.1.1.2.0/09/APIA/VIAA/044

Thanks

for your attention!